

**IRIDIUM BASED MIXED OXIDES AS EFFICIENT ANODE  
CATALYSTS FOR SOLID POLYMER ELECTROLYTE  
(SPE) ELECTROLYSERS**

by

**Cecil Felix**



Submitted in fulfilment of the requirements for the degree of

Masters in Chemistry

Department of Chemistry,

University of the Western Cape

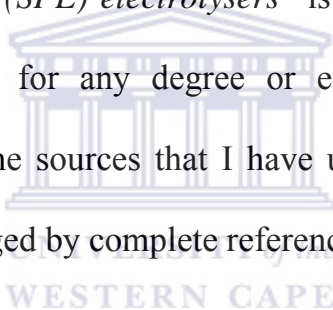
Supervisor: Prof Vladimir M. Linkov

Co supervisor: Dr Sivakumar Pasupathi

November 2009

## **Declaration**

I declare that “*Iridium based mixed oxides as efficient anode catalysts for solid polymer electrolyte (SPE) electrolysers*” is my own work and that it has not been submitted for any degree or examination in any other university, and that all the sources that I have used or quoted have been indicated and acknowledged by complete references



Cecil Felix

November, 2009

Signed.....

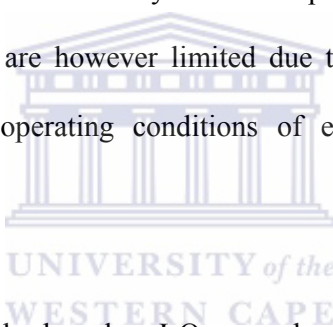
## ***Acknowledgements***

- I firstly thank God Almighty for his love and grace that I have experienced and for being the driving force in my life
- A special thank you goes to Jolene, my wife, for her love and support throughout the duration of the research
- A special thank you goes to my parents who have given me so much and always supported me in my undertakings
- I am very grateful to Prof. Vladimir Linkov and the staff of the South African Institute for Advanced Material Chemistry for allowing me to conduct my research, as well as for financial support
- A special thank you also goes to Dr. Sivakumar Pasupathi for his guidance and assistance throughout the duration of the research
- Thank you to Adrian Josephs (Department of Physics, UWC) for SEM and TEM characterization of my samples
- Thank you to Dr. Remy Bucher (Materials Research Group, iThemba Labs) for X-ray diffraction characterization of all samples
- Thank you to the National Research Foundation (NRF) for financial assistance
- A warm thanks is offered to my fellow colleagues who created a friendly work environment.

## **Abstract**

The objective of the thesis is to develop highly efficient catalysts for solid polymer electrolyte (SPE) electrolyser anodes.

The anode is the primary cause of the large overpotential of SPE electrolysers and also adds significantly to the cost of the electrolysers. Currently, unsupported IrO<sub>2</sub> is a widely used anode catalyst as it exhibits the best stability during the oxygen evolution reaction. The activity of IrO<sub>2</sub> needs to be improved significantly to address the high cost and efficiency issues of the SPE electrolyser. Developments aimed at improving the activity of unsupported IrO<sub>2</sub> are however limited due to the limitations of the well-known supports under the operating conditions of electrolysers, leading to their oxidation.



In this study binary metal oxides based on IrO<sub>2</sub> were developed and optimized as anode catalysts for the SPE electrolyser and compared to the ‘state-of-art’ commercial IrO<sub>2</sub> catalyst. The Adams fusion method was adapted and used to synthesize the catalysts. The activities of the catalysts were determined using half-cell studies. Optimum conditions for the preparation of unsupported IrO<sub>2</sub> catalysts were found to be 350 °C and 2 hours. The resulting catalysts had twice the activity of the ‘state-of-art’ commercial IrO<sub>2</sub> catalyst. Secondary metals were carefully selected, after carrying out both a literature study and an experimental study. Binary metal oxides were then developed using the optimum synthesis conditions. Four binary metal oxides were studied to identify the best/most efficient catalyst for electrolysis.

The catalysts were characterized using XRD, TEM, SEM and EDS analyses, in efforts to understand and correlate the activity of the catalysts to its physical properties and obtain information that could be useful for the further development of efficient catalysts.

Although all the binary metal oxides studied showed improved activity compared to IrO<sub>2</sub>, the catalytic activity of Ir<sub>0.7</sub>Ru<sub>0.3</sub>O<sub>2</sub> was found to be significantly better than the commercial catalyst: it was over 5 times more active than the ‘state-of-art’ commercial IrO<sub>2</sub> catalyst. Ir-Pd mixed oxides also proved to be highly efficient as anode catalysts for SPE electrolysers.



## ***List of figures***

<b>Figure 1.1:</b> Schematic diagram of a hydrogen energy cycle .....	2
<b>Figure 1.2:</b> Schematic diagram of the cross-section of a SPE electrolyser .....	9
<b>Figure 1.3:</b> A photograph of prepared MEAs .....	10
<b>Figure 1.4:</b> Chemical structure of the Nafion membrane .....	12
<b>Figure 1.5:</b> Volcano plot of the HER on various metals.....	13
<b>Figure 1.6:</b> A proposed scheme of the oxygen evolution reaction on conductive metal oxide anodes .....	16
<b>Figure 4.1:</b> Catalytic activity of in-house IrO <sub>2</sub> at 1.8 V (500 °C, 0.5–4 hours).....	40
<b>Figure 4.2:</b> Peak catalytic activity of in-house IrO <sub>2</sub> at 1.8 V (500 °C, 0.5–4 hours) .....	41
<b>Figure 4.3:</b> XRD patterns of in-house IrO <sub>2</sub> (500 °C, 0.5–4 hours) .....	42
<b>Figure 4.4:</b> TEM images of in-house IrO <sub>2</sub> (500 °C, 0.5–4 hours) .....	43
<b>Figure 4.5:</b> Catalytic activity of in-house IrO <sub>2</sub> at 1.8 V (2 hours, 250–500 °C).....	45
<b>Figure 4.6:</b> Peak catalytic activity of in-house IrO <sub>2</sub> at 1.8 V (2 hours, 250–500 °C).....	45
<b>Figure 4.7:</b> XRD patterns of in-house IrO <sub>2</sub> (2 hours, 250–500 °C) .....	46
<b>Figure 4.8:</b> TEM images of in-house IrO <sub>2</sub> (2 hours, 250–500 °C) .....	47
<b>Figure 4.9:</b> Catalytic activity of commercial and best in-house IrO <sub>2</sub> at 1.8 V (glassy carbon working electrode).....	48
<b>Figure 4.10:</b> XRD patterns of commercial and best in-house IrO <sub>2</sub> .....	49
<b>Figure 4.11:</b> SEM images of commercial and best in-house IrO <sub>2</sub> .....	49
<b>Figure 4.12:</b> TEM images of commercial and best in-house IrO <sub>2</sub> .....	50
<b>Figure 4.13:</b> Catalytic activity of commercial and best in-house IrO <sub>2</sub> at 1.8 V (catalyst coated titanium mesh working electrode).....	51
<b>Figure 4.14:</b> Catalytic activity of Ir-Ru mixed oxides, commercial and best in-house IrO <sub>2</sub> at 1.8 V .....	53
<b>Figure 4.15:</b> Peak catalytic activity of Ir-Ru mixed oxides, commercial and best in- house IrO <sub>2</sub> at 1.8 V .....	53
<b>Figure 4.16:</b> XRD patterns of Ir <sub>0.7</sub> Ru <sub>0.3</sub> O <sub>2</sub> .....	54

<b>Figure 4.17:</b> SEM image of Ir <sub>0.7</sub> Ru <sub>0.3</sub> O <sub>2</sub> .....	55
<b>Figure 4.18:</b> TEM image of Ir <sub>0.7</sub> Ru <sub>0.3</sub> O <sub>2</sub> .....	55
<b>Figure 4.19:</b> Catalytic activity of Ir-Sn mixed oxides, commercial and best in-house IrO <sub>2</sub> at 1.8 V.....	56
<b>Figure 4.20:</b> Peak catalytic activity of Ir-Sn mixed oxides, commercial and best in-house IrO <sub>2</sub> at 1.8 V.....	57
<b>Figure 4.21:</b> XRD patterns of Ir <sub>0.9</sub> Sn <sub>0.1</sub> O <sub>2</sub> .....	58
<b>Figure 4.22:</b> SEM image of Ir <sub>0.9</sub> Sn <sub>0.1</sub> O <sub>2</sub> .....	59
<b>Figure 4.23:</b> TEM image of Ir <sub>0.9</sub> Sn <sub>0.1</sub> O <sub>2</sub> .....	59
<b>Figure 4.24:</b> Catalytic activity of Ir-Ta mixed oxides, commercial and best in-house IrO <sub>2</sub> at 1.8 V.....	60
<b>Figure 4.25:</b> Peak catalytic activity of Ir-Ta mixed oxides, commercial and best in-house IrO <sub>2</sub> at 1.8 V.....	60
<b>Figure 4.26:</b> XRD patterns of Ir <sub>(0.8)</sub> Ta <sub>(0.2)</sub> O <sub>x</sub> .....	61
<b>Figure 4.27:</b> SEM image of Ir <sub>(0.8)</sub> Ta <sub>(0.2)</sub> O <sub>x</sub> .....	62
<b>Figure 4.28:</b> TEM image of Ir <sub>(0.8)</sub> Ta <sub>(0.2)</sub> O <sub>x</sub> .....	62
<b>Figure 4.29:</b> Catalytic activity of Ir-Pd mixed oxides, commercial and best in-house IrO <sub>2</sub> at 1.8 V.....	63
<b>Figure 4.30:</b> Peak catalytic activity of Ir-Pd mixed oxides, commercial and best in-house IrO <sub>2</sub> at 1.8 V.....	64
<b>Figure 4.31:</b> XRD patterns of Ir <sub>(0.7)</sub> Pd <sub>(0.3)</sub> O <sub>x</sub> .....	65
<b>Figure 4.32:</b> SEM image of Ir <sub>(0.7)</sub> Pd <sub>(0.3)</sub> O <sub>x</sub> .....	66
<b>Figure 4.33:</b> TEM image of Ir <sub>(0.7)</sub> Pd <sub>(0.3)</sub> O <sub>x</sub> .....	66
<b>Figure 4.34:</b> Peak catalytic activity of the best metal oxide catalysts at 1.8 V.....	67

### **List of tables**

<b>Table 3.1:</b> Chemicals used for metal oxide catalyst preparation.....	33
<b>Table 3.2:</b> Chemicals used for anode preparation.....	33
<b>Table 4.1:</b> Effect of reaction time on the particle size of IrO <sub>2</sub> .....	42
<b>Table 4.2:</b> Effect of temperature on the particle size of IrO <sub>2</sub> .....	47

### ***List of abbreviations***

<b>CCM</b>	Catalyst coated membrane
<b>CV</b>	Cyclic voltammetry
<b>DSA</b>	Dimensionally stable anode
<b>EDS</b>	Energy dispersive spectroscopy
<b>EIS</b>	Electrochemical impedance spectroscopy
<b>HER</b>	Hydrogen evolution reaction
<b>MEA</b>	Membrane electrode assembly
<b>OER</b>	Oxygen evolution reaction
<b>PCM</b>	Proton conducting membrane
<b>PEM</b>	Proton exchange membrane
<b>RHE</b>	Reversible hydrogen electrode
<b>SEM</b>	Scanning electron microscopy
<b>SHE</b>	Standard hydrogen electrode
<b>SOE</b>	Solid oxide electrolyte
<b>SPE</b>	Solid polymer electrolyte
<b>TEM</b>	Transmission electron microscopy
<b>UPD</b>	Underpotential deposition
<b>XPS</b>	X-ray photoelectron spectroscopy
<b>XRD</b>	X-ray diffraction
<b>YSZ</b>	Yttrium stabilized zirconia

### ***List of symbols***

$E^0$	Standard potential (V)
$i_0$	Exchange current density ( $A\ cm^{-2}$ )
$\Delta G_f^0$	Standard Gibbs free energy ( $kJ\ mol^{-1}$ )



## Table of contents

<b>Declaration</b> .....	<b>ii</b>
<b>Acknowledgements</b> .....	<b>iii</b>
<b>Abstract</b> .....	<b>iv</b>
<b>List of figures</b> .....	<b>vi</b>
<b>List of tables</b> .....	<b>vii</b>
<b>List of abbreviations</b> .....	<b>viii</b>
<b>List of symbols</b> .....	<b>viii</b>
<b>Chapter 1: Introduction</b> .....	<b>1</b>
1.1 Hydrogen as a future energy carrier .....	1
1.2 Hydrogen production via the electrolysis of water.....	2
1.3 An overview of electrolyser technology.....	4
1.3.1 Alkaline electrolyser.....	4
1.3.2 Solid oxide electrolyte electrolyser .....	5
1.3.3 Solid polymer electrolyte electrolyser.....	6
1.4 Background to solid polymer electrolyte electrolysers .....	7
1.4.1 Principle of operation of the solid polymer electrolyte electrolyser .....	8
1.4.2 Membrane electrode assembly .....	10
1.4.3 The proton conducting membrane.....	11
1.5 Electrode reactions in solid polymer electrolyte water electrolysis	13
1.5.1 Hydrogen evolution reaction .....	13
1.5.2 Oxygen evolution reaction.....	14
1.6 Shortcomings .....	17
1.7 Objectives .....	17
<b>Chapter 2: Literature review</b> .....	<b>20</b>
2.1 Solid polymer electrolyte water electrolysis for hydrogen production	
.....	20

2.2 Metal oxides as anode catalysts for solid polymer electrolyte electrolysers .....	25
2.2.1 IrO <sub>2</sub> as anode catalyst .....	25
2.2.2 Ir-Sn mixed oxides as anode catalysts .....	26
2.2.3 Ir-Ru mixed oxides as anode catalysts .....	27
2.2.4 Ir-Ta mixed oxides as anode catalysts .....	29
2.2.5 Ir-Pd mixed oxides as anode catalysts .....	30
2.3 Conclusion .....	31
<b>Chapter 3: Experimental .....</b>	<b>33</b>
3.1 Chemicals and apparatus .....	33
3.2 Metal oxide preparation .....	34
3.2.1 Optimization of the preparation conditions of IrO <sub>2</sub> .....	34
3.2.2 Preparation of binary metal oxides .....	35
3.3 Preparation of the working electrode (anode) .....	35
3.3.1 Glassy carbon working electrode .....	35
3.3.2 Catalyst coated titanium mesh working electrode .....	36
3.4 Electrochemical characterization of the catalysts .....	36
3.4.1 Electrochemical cell setup .....	36
3.4.2 Electrochemical measurements .....	37
3.5 Physiochemical characterization of the catalysts .....	37
3.5.1 Scanning electron microscopy .....	37
3.5.2 Transmission electron microscopy .....	37
3.5.3 X-ray diffraction .....	38
<b>Chapter 4: Results and discussion .....</b>	<b>40</b>
4.1 Optimization of the IrO <sub>2</sub> catalyst .....	40
4.1.1 Effect of reaction time on the activity of IrO <sub>2</sub> .....	40
4.1.2 Effect of temperature on the activity of IrO <sub>2</sub> .....	44
4.2 Comparison of in-house and commercial IrO <sub>2</sub> .....	48
4.3 Binary metal oxides as anode catalysts for solid polymer electrolyte electrolysers .....	51

4.3.1 Ir-Ru mixed oxides as anode catalysts .....	52
4.3.2 Ir-Sn mixed oxides as anode catalysts.....	55
5.3.3 Ir-Ta mixed oxides as anode catalysts.....	59
4.3.4 Ir-Pd mixed oxides as anode catalysts.....	62
4.3.5 Summary of the best catalysts .....	66
<b><i>Chapter 5: Conclusions and recommendations</i></b> .....	<b>68</b>
5.1 Conclusions.....	68
5.2 Recommendations.....	69
<b><i>References</i></b> .....	<b>70</b>



## ***Chapter 1: Introduction***

### ***1.1 Hydrogen as a future energy carrier***

Fossil fuels have played, and are playing, a major role in shaping and forming the world we see around us today. Fossil fuels are hydrocarbon based, and are most widely available as oil, coal and natural gas. By drilling and/or digging into the earth's surface oil can be removed, and then processed into products such as diesel, petroleum and various other organic products. Petrol and diesel are the two main fuels used to power automobiles. However, the combustion of these fuels emits greenhouse gases that are harmful to the environment. The release of CO<sub>2</sub> to the atmosphere and its impact on global warming has led to worldwide concerns and an international agreement on the reduction of CO<sub>2</sub> (Kyoto Protocol) [1, 2, 3]. Oil has played, and continues to play, a major role in various political issues since oil supplies are not evenly distributed and many countries are dependent on others for oil. Energy demand is also increasing continuously due to the rapid increase in the population and industrialization. The development of energy sources is however not keeping up with the pace of energy consumption. Another major problem associated with fossil fuels is that resources are limited; it is estimated that oil reserves will start to become depleted by 2050 [3]. If no suitable alternative energy source is found we will soon find ourselves in a global energy crisis.

In recent years hydrogen has received considerable attention since many scientists across the globe see it as the most suitable energy carrier to provide us with energy in the future. Hydrogen, when generated from renewable energy sources such as wind, solar, hydro, geothermal, etc., is virtually pollution free: the only by-product is water.

Hydrogen used as a fuel has benefits over the hydrocarbon rich fuels: it has a higher specific energy density by mass and does not present the problem of the emission of pollutants or greenhouse gases, such as CO<sub>2</sub> [4]. There are various ways of producing hydrogen, such as steam reforming, coal gasification and electrolysis of water, and obtaining hydrogen from biomass. Currently, about 98% of the world's hydrogen is produced by steam reforming: steam is used to produce hydrogen from methane typically derived from natural gas [4, 5]. Today steam reforming is the most cost effective method for producing hydrogen, however, natural gas is not a renewable energy source and it contributes to the emission of CO<sub>2</sub>. Figure 1.1 illustrates a hydrogen energy system where renewable energy sources are used to produce hydrogen via the electrolysis of water, with the only by-product being water.

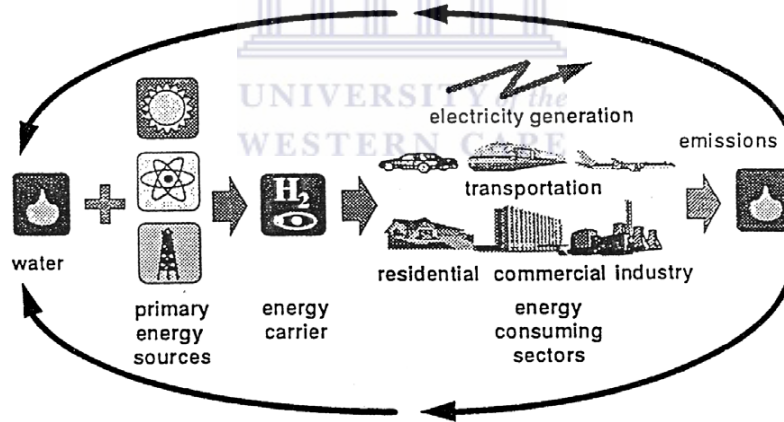


Figure 1.1: Schematic diagram of a hydrogen energy cycle [6].

## 1.2 Hydrogen production via the electrolysis of water

Electrolysis involves the passing of an electrical current through two electrodes to split water into hydrogen and oxygen. Hydrogen produced via electrolysis of water is

usually of very high purity [4, 7]. The reaction to dissociate water into hydrogen and oxygen are given by equation 1.1 [5]:



The reaction will occur on any conductive surface when sufficient energy is supplied. Certain materials, such as high surface area metals, are more efficient and consume less energy than non-metallic materials to produce a given quantity of hydrogen.

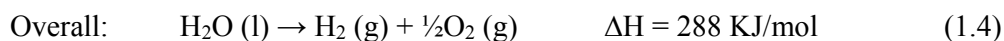
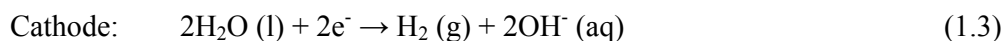
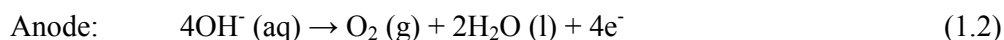
The electrolysis of water was discovered in 1789 by Adriaan Paets van Trootswijk and Johan Rudolf, in Amsterdam; they found that water could be split into its constituent elements by electric power. Electrolysis of water was later brought into the public eye by Nicholson and Carlisle in 1800. The first commercial splitting of water to produce hydrogen and oxygen dates back to the 1890s. By 1902 more than 400 industrial water electrolyzers were in operation [1] and by 1939 the first large water electrolysis plant with a capacity of 10,000 Nm<sup>3</sup> H<sub>2</sub>/h was in operation [8].

There are different types of electrolyzers, which can be distinguished by the type of electrolyte and materials used for the electrodes. Today most commercial electrolyzers use an alkaline electrolyte. However, electrolyzers using a solid polymer electrolyte (SPE) and electrolyzers using a solid oxide electrolyte (SOE) have recently received considerable attention because they offer the possibility of achieving higher energy efficiencies.

## 1.3 An overview of electrolyser technology

### 1.3.1 Alkaline electrolyser

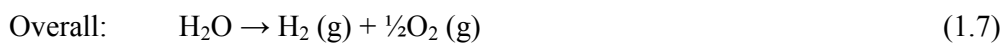
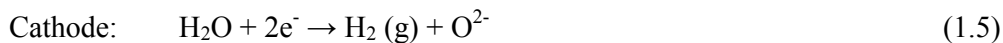
Most commercial electrolysers in operation make use of a strongly alkaline aqueous electrolyte of approximately 30% KOH or NaOH [7, 9], in which the hydroxide ions ( $\text{OH}^-$ ) are the charge carriers, to maximize the ion conductivity [10]. These systems are well established and are used in various industrial processes. One of the advantages of the alkaline electrolyser is that it makes use of relatively inexpensive electrode and construction materials [11]. Alkaline electrolysers use nickel coated with a film of platinum as the cathode catalyst and nickel or copper coated with metal oxides (Mn, Ru or W) for the anode catalyst. The liquid electrolyte is consumed in the reaction and should be replenished over time [7]. The disadvantage of this technology is that it has low specific production rates, high energy consumption and voluminous systems [11]. Alkaline electrolysers show low energy efficiency because of the high overpotential of the oxygen evolving anodes. Low pressure alkaline electrolysers are mainly built in monopolar tanks, which are the simplest construction principle, whereas high pressure units are built in the bipolar filter press arrangement to save space [8]. Alkaline electrolyser units have typical current densities of 100–300  $\text{mA cm}^{-2}$  with operating efficiencies of 50–60% based on the lower heating value of hydrogen [7, 11]. The electrode reactions that take place in such systems are given by equations 1.2–1.4 [7, 10]:



Advanced alkaline electrolyzers are now in use because of their advantageous features. These systems can achieve efficiencies as high as 73%, based on the higher heating value of hydrogen [10].

### **1.3.2 Solid oxide electrolyte electrolyser**

The first solid oxide electrolyte (SOE) electrolyser was developed in 1972 [8] but during the 1990s further developments were slow because of the low fossil fuel prices. More recently it has however received renewed attention, as its use offers a green energy technology [12]. Operating at higher temperatures (typically 600–1000 °C), the operating efficiencies of the SOE electrolyser are increased because of the decrease in the anode and cathode overpotentials [13]. The SOE electrolyser also uses a solid electrolyte, which, unlike the alkaline electrolyser, is noncorrosive, and does not have any liquid and flow distribution problems. Costly materials and fabrication methods are however required because of the high operating temperatures. A heat source is also required. The materials are similar to those developed for the solid oxide fuel cell, namely an yttrium stabilised zirconia (YSZ) as electrolyte, a nickel containing YSZ as anode, and a cathode made from lanthanum [7]. In a SOE electrolyser the following takes place: water is supplied to the cathode, oxygen is transported through the electrolyte and hydrogen is produced at the cathode. The electrode reactions that take place in such systems are given by equations 1.5–1.7 [14]:





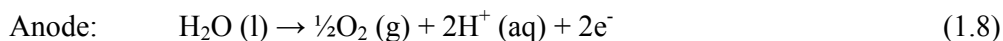
The efficiency of a SOE electrolyser depends on the operating temperature. Efficiencies based on electrical input alone are reported to be between 85 and 90%.

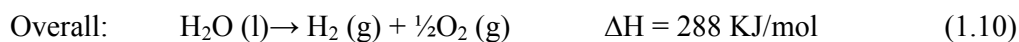
### **1.3.3 Solid polymer electrolyte electrolyser**

Solid polymer electrolyte (SPE) electrolysers, also known as proton exchange membrane (PEM) electrolysers, have received considerable attention in recent years. The technology is based on recent advances in PEM fuel cell technology. The SPE is most commonly a Nafion membrane, developed by Du Pont (USA) [7, 15]. SPE electrolyser technology was first proposed by the General Electric Company (USA) and was more recently (1976–1989) developed by ABB, Switzerland [8, 16]. Some of the advantages of the SPE electrolyser over the alkaline electrolyser [8] are the following:

- greater safety and reliability, since there is no need to circulate a caustic electrolyte
- the membrane can withstand high differential pressure without damage and is effective in preventing gas mixing.

A SPE electrolyser requires expensive noble metals such as Pt black, IrO<sub>2</sub> and Ru as catalysts. SPE electrolyser units can typically operate at high current densities (1–2 A cm<sup>-2</sup>) [11] and achieve energy efficiencies of 55–70% [7]. The half-cell electrode reactions are given by equations 1.8–1.10 [7, 10]:





### **1.4 Background to solid polymer electrolyte electrolyzers**

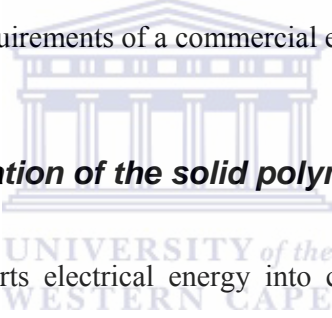
Recently, the use of SPE electrolyser systems has gained significant attention as a method for the production of carbon-free hydrogen [17, 18]. SPE electrolyzers offer the possibility of converting electrical energy to chemical energy, in the form of hydrogen, which can be stored and then converted back to electrical energy (via a fuel cell) when needed [11]. It is expected that in the future hydrogen will become the most attractive energy carrier and the electrolysis of water will be the most practical and efficient process for producing hydrogen.

The first SPE electrolyser was developed in 1966 by the General Electric Company (USA) for space applications [8, 16, 19–21]. These units were initially developed to provide oxygen for aerospace and submarines but the design could readily be adapted and upscaled to large hydrogen generation plants. Today SPE electrolyzers are used in producing high purity hydrogen for fuel cells, hydrogen welding, metallurgy of especially pure metals and alloys, manufacture of pure substances for the electronics industry, analytical chemistry, etc [19].

SPE electrolyzers offer several advantages over the traditional alkaline electrolyzers: they have higher energy efficiency and specific production capacity, the system is simple and safe, and maintenance requirements are low [22]. Other favourable features of SPE electrolyzers include ecological cleanliness, the production of high purity gases, and the possibility of directly obtaining compressed gases in an installation, with a greater level of safety [19]. The main disadvantage is the high cost,

which is mainly due to components such as expensive electrodes, the proton conducting membranes (PCM) and the bipolar plates [11, 22].

The oxygen evolution electrode (anode) is the greatest source of overpotential of the system at a typical operating current density [17] and therefore the anode catalyst needs to be highly stable and active. Anode catalysts are therefore most commonly made from expensive noble metals as these exhibit the highest stability and activity during the oxygen evolution reaction (OER). Non-noble metals corrode under the reactions conditions and are thus not suitable as catalysts for use as electrodes for the SPE electrolyser. The Nafion membrane, developed by Du Pont (USA) [7, 15], is most commonly used as the SPE. The Nafion membrane is a perfluorinated membrane that fulfils the requirements of a commercial electrolyser system [23].



#### ***1.4.1 Principle of operation of the solid polymer electrolyte electrolyser***

The SPE electrolyser converts electrical energy into chemical energy by splitting water to its constituents, hydrogen and oxygen. The gases can then be stored in suitable containers. Hydrogen can be stored either as a gas, a liquid or in metal hydrides. The stored hydrogen can then be directly burned inside an internal combustion engine or used in a fuel cell to power automobiles, aircraft and spacecraft, as well as to provide electrical energy in rural areas or during peak demands. Hydrogen produced via an SPE electrolyser is however only truly clean when the electricity needed to run the SPE electrolyser is generated by renewable sources, such as wind, solar, or hydro power. The electricity can be supplied during off-peak times when extra electricity is available. The SPE electrolyser consists mainly of a PCM, anode and cathode catalysts, and bipolar plates [11].

The reaction takes place at the membrane electrode assembly (MEA), which is considered as the heart of the SPE electrolyser [24]. The MEA consists of the anode and cathode catalyst, and the PCM. The anode and cathode are situated on each side of the PCM. Electrical contact and mechanical support are established with porous backings like metallic meshes or sinters [25]. Figure 1.2 shows a schematic of the cross-section of a single cell SPE electrolyser.

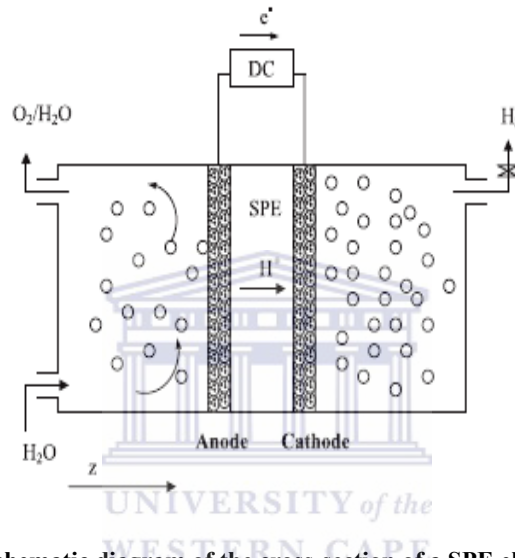


Figure 1.2: Schematic diagram of the cross-section of a SPE electrolyser [24].

Water is introduced at the anode side, which is connected to a power source. A potential is then applied to the anode, which splits the water into protons, electrons and oxygen. Reactions that occur at the electrodes are illustrated by equations 1.8–1.10 [15, 24, 26] as was discussed in section 1.3.3:



The oxygen produced is removed and stored using a suitable method, while solvated protons permeate through the PCM to the cathode side. Electrons follow a path via an external circuit to the cathode and recombine with the protons to form hydrogen gas.



### 1.4.2 Membrane electrode assembly

The membrane electrode assembly (MEA) is the core part of the SPE electrolyser and electrochemical reactions only take place at the 'triple phase boundary' where the reaction materials, electrolyte and catalysts are in contact [21]. A photograph of different sizes of MEAs prepared by my colleagues is shown in Figure 1.3.

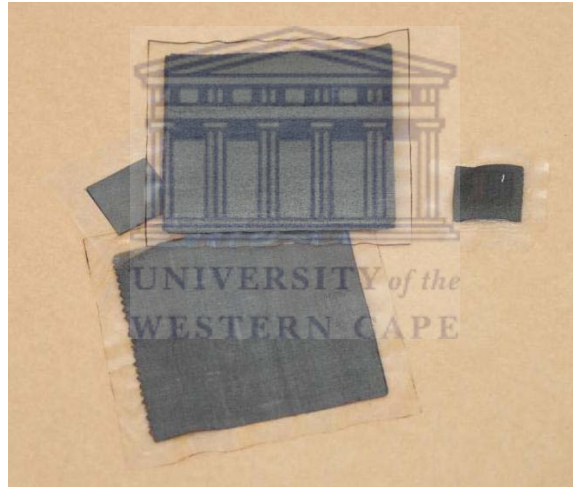


**Figure 1.3: A photograph of prepared MEAs.**

A high performance MEA could be obtained by improving the contact between the electrolyte and the catalyst layers [27]. The MEA thus essentially consists of the PCM with the anode catalyst and cathode catalyst contacted on opposite sides. It is therefore important that the interface between the membrane and the catalysts be as large as possible and the contact resistance as low as possible [28]. There are currently various methods of MEA preparation: chemical plating [29, 30], a decal transfer method [21], and a catalyst-coated membrane (CCM) technique [21, 31].

Chemical plating results in MEAs that have large catalyst particle diameters and low surface areas, leading to a high catalyst loading. These factors result in MEAs with a low overall performance. The decal transfer method and the CCM technique reduce the required catalyst loading and enhance the adhesion between the PCM and the catalyst layers, thereby improving the subsequent performance of the MEA for water electrolysis [21].

### ***1.4.3 The proton conducting membrane***

The proton conducting membrane (PCM) used for SPE electrolyzers is most commonly a Nafion membrane (Du Pont, USA) [7, 15]. Nafion membranes are perfluorinated sulphonic acid cation exchange membranes, which offer the stability (chemically and mechanically) and performance required for long-term operation of the electrolyser [23]. Nafion membranes also find application in other energy related fields, such as fuel cells [26], hydrogen compressors and solar cell systems. During the electrolysis of water the PCM serves as a solid electrolyte that conducts protons and also serves as a separator of the produced gases. These membranes are however known to be chemically unstable at temperatures above 100 °C [22]. The chemical structure of the Nafion membrane is illustrated in Figure 1.4.

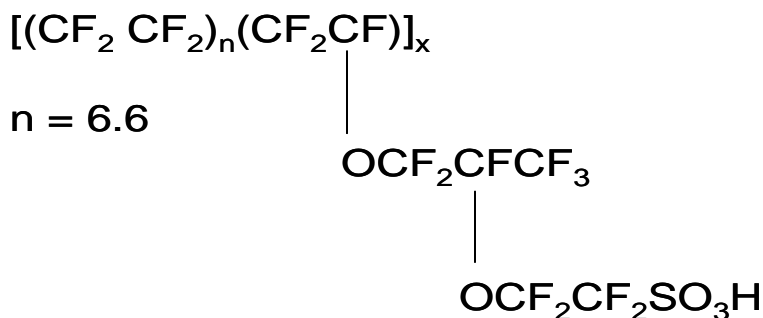
**Nafion Du Pont<sup>®</sup>**

Figure 1.4: Chemical structure of the Nafion membrane [1].

When the membrane is saturated with water it becomes an excellent ionic conductor. Ion conduction is brought about by the mobility of protons, which pass from one sulphonic acid group to the other due to the presence of water. The sulphonic acid groups do not move and hence the acid concentration of the membrane remains constant [23]. The acidity of the Nafion membrane is similar to that of a 20 wt % H<sub>2</sub>SO<sub>4</sub> solution [16], thus the catalysts used should be acid resistant. Noble metals such as the platinum group metals are acid resistant and are widely used as catalysts. The main disadvantage of the Nafion membranes is the high cost [11, 22]. However SPE electrolyzers offer more advantages than disadvantages, such as [23]:

1. Operation at high differential pressures (> 68 atm), resulting in the production of pressurized gases, thus eliminating the additional step of gas compression
2. Use of a fixed electrolyte, which means that there is no caustic liquid circulating through the system
3. Elimination of acid mixing with the produced gases, i.e. oxygen and hydrogen
4. A constant electrolyte concentration during cell operation
5. Low cell maintenance.

In practice, however, the permeability of the Nafion membrane to hydrogen and oxygen increases significantly with increasing temperature and pressure [32, 33]. This leads to cross-contamination, which in turn could lead to explosive H<sub>2</sub>/O<sub>2</sub> gas mixtures. Thus it is necessary to develop a membrane with low permeability to hydrogen and oxygen for use in high temperature and pressurized electrolyser units [32].

## 1.5 Electrode reactions in solid polymer electrolyte water electrolysis

### 1.5.1 Hydrogen evolution reaction

The standard potential of hydrogen is, by definition, zero. A volcano plot is used to compare the electrochemical activity of the hydrogen evolution reaction (HER) on various metals. In the volcano plot  $\log(i_0)$  is related to the bond energy of chemisorbed hydrogen to the metal [1, 34]. A well-known electrode kinetics example is the plot reported by Trasatti, illustrated in Figure 1.5 [35].

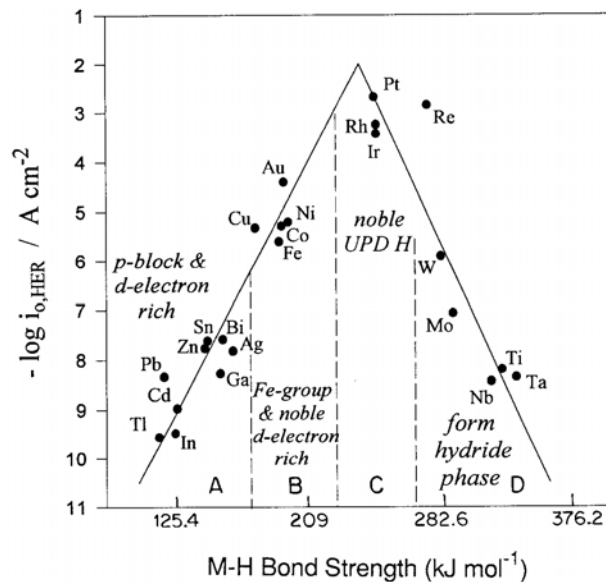


Figure 1.5: Volcano plot of the HER on various metals [35].



The volcano plot shows the following: for the metals on the left hand side of the curve, with low bond strength, the adsorption of hydrogen becomes the rate-determining step, and for the metals on the right hand side of the curve, with strong bond strength, the desorption of hydrogen becomes the rate-determining step. Thus, metals with intermediate bond strengths, which are the noble metals, are the most active toward the HER [35]. Platinum provides the best performance for the HER and is commonly used as the cathode catalyst in SPE electrolyzers [24]. It is also well known from hydrogen evolution studies that metal alloys consisting of elements on both sides of the volcano plot may give rise to synergistic effects [11, 36].

### **1.5.2 Oxygen evolution reaction**

The oxygen evolution reaction (OER) takes place in many industrial processes, such as water electrolysis, electrowinning, cathodic protection and electro-organic synthesis [37]. Unlike hydrogen and chlorine evolution on metals or metal oxides, the OER represents low reversibility. Understanding the complicated kinetics of the OER presents a challenge to electrochemists [38]. Metal oxides are most frequently used as anodes in acidic media, although most transition metal oxides such as nickel, cobalt and manganese undergo corrosion under these conditions. The cations of these metals are known to poison the membrane by attaching to the sulphonic acid groups, thereby reducing the conductivity of the membrane [39]. These cations also strongly adsorb to the active sites of the platinum cathode, further deactivating the electrode. Platinum group metal oxides such as  $\text{RuO}_2$  and  $\text{IrO}_2$ , and some transition metal oxides such as  $\text{PbO}_2$  and  $\text{SnO}_2$ , have been found to be more stable during the OER. The standard potential for OER is  $1.23 \text{ V}_{\text{RHE}}$  (RHE, reversible hydrogen electrode), which falls

above the standard potential of almost all solid materials, explaining why only a few materials are stable under the OER [1].

The OER is a complex reaction and involves pathways of high activation energy and energetic intermediates [40]. Oxygen species cover the surface of bare metals by underpotential deposition (UPD), by discharge of water before the liberation of oxygen, and since the M–O bond strength (M: metal) is always stronger than the O–O dissociation energy, the OER always takes place at a metal oxide surface [1]. Fierro *et al.* [37] proposed that in acidic media the mechanism of the OER involves two parallel reaction paths. First there is discharge of the water molecules at the metal oxide surface,  $\text{MO}_x$ , to form adsorbed hydroxyl radicals [eq. 1.14]:



A second step depends on the nature of the interaction between the metal oxide and the electrogenerated hydroxyl radicals. They distinguished two limiting cases, i.e. oxygen evolution via physisorbed hydroxyl radicals and via chemisorbed intermediates. In the first case the physically adsorbed hydroxyl radicals are electrochemically oxidized to form oxygen, involving hydrogen peroxide as an intermediate [eq. 1.15]:



In the second case the chemisorbed hydroxyl radicals react with the oxide to form the higher oxide [eq. 1.16]:



The higher oxide then decomposes to regenerate the lower oxidation state and evolves oxygen [eq. 1.17]:



A schematic representation of the OER is illustrated in Figure 1.6.

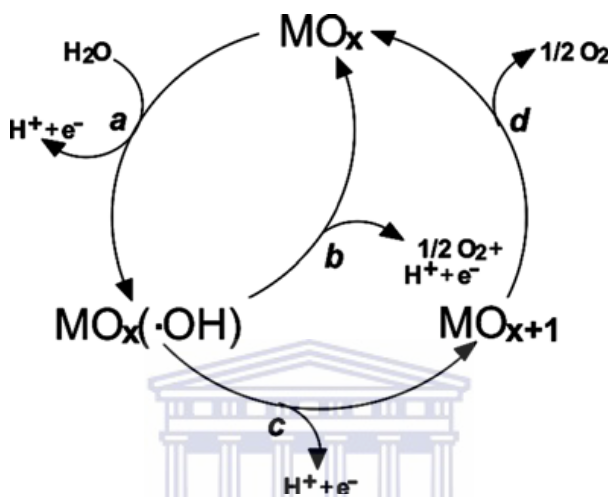
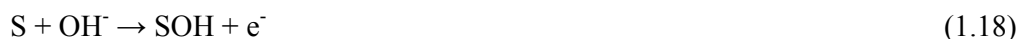


**Figure 1.6:** A proposed scheme of the oxygen evolution reaction on conductive metal oxide anodes: (a) formation of adsorbed hydroxyl radicals by water discharge, (b) oxygen evolution by electrochemical oxidation of physisorbed hydroxyl radicals, (c) formation of the higher metal oxide via chemisorbed hydroxyl radicals and (d) oxygen evolution by chemical decomposition of the higher oxide [37].

A more general scheme for the mechanism of the OER as suggested by Krasil'shchikov can be written as follows [41–43]:



where S represents a catalytically active site for the reaction.

## **1.6 Shortcomings**

The first SPE electrolyzers were developed by the General Electric Company in 1966 [8, 16, 19–21]. SPE electrolyzers are currently being developed for special purposes, such as space and marine applications. SPE electrolyzers have advantages over the traditional alkaline electrolyser technology and also create new options for the fuel cell system, such as a regenerative fuel cell, which operates both as a fuel cell and as an electrolyser [24]. However, an industrial scale SPE electrolyser is not yet a reality because of the high production costs of the SPE electrolyser components. These components mainly include the PCMs, the anode and cathode catalysts and the bipolar plates. In this study we mainly focused on the development of an anode catalyst that has higher activity and stability than that of the ‘state-of-art’ commercial IrO<sub>2</sub> catalyst. The anode is the greatest source of overpotential and thus the catalyst should be stable as well as highly active under the OER. IrO<sub>2</sub> is most commonly used as anode catalyst as it shows the greatest stability during the OER. IrO<sub>2</sub> is very expensive, adding significantly to the cost of the electrolyser. Reductions in component costs can lead to a reduction in the cost of SPE electrolyzers by up to 40%, promoting their commercialization.

## **1.7 Objectives**

The main objective of this study is to develop an anode catalyst that has higher activity and greater stability than the ‘state-of-art’ commercial IrO<sub>2</sub> catalyst. A more active and stable catalyst will offer the following advantages [1]:

- The requirement of lower quantities of noble metals
- Higher energy efficiency
- Higher specific production capacity

- Longer lifetime.

The specific objectives are the following:

- (1) The Adams fusion method will be adapted and then used to prepare the catalysts.
- (2) The catalyst preparation conditions will be optimized to improve the catalytic activity of  $\text{IrO}_2$  and will then be further improved by incorporating secondary metal oxides such as those of ruthenium, tin, tantalum and palladium.
- (3) The electrochemical activities of the prepared catalysts will be evaluated and compared to the activity of the commercial  $\text{IrO}_2$  catalyst.
- (4) The catalysts will be characterized, using X-ray diffraction (XRD), scanning electron microscopy (SEM), transmission electron microscopy (TEM) and energy dispersive spectroscopy (EDS), in efforts to understand and correlate the activity of the catalysts to its physical properties, and obtain information that could be useful for the further development of efficient catalysts.

The addition of secondary metal oxides, such as the oxides of tin, ruthenium, tantalum and platinum, to  $\text{IrO}_2$ , has been researched by various groups and some interesting results have been obtained. There are various factors that determine how well these metal oxides perform as catalysts, for example: the production method and conditions, size of the particles, molar ratio of metal oxides, etc. The most common methods used to prepare these metallic oxides include the following:

- (i) The polyol method, which involves the reduction of metal precursors in ethylene glycol.

- (ii) A thermal decomposition method, used to prepare the well known dimensionally stable anodes (DSAs).
- (iii) The Adams fusion method, which is the fusion of metal precursors with  $\text{NaNO}_3$ .



## **Chapter 2: Literature review**

### **2.1 Solid polymer electrolyte water electrolysis for hydrogen production**

The first SPE electrolyser was developed by the General Electric Company in 1966 [8, 6, 19–21] for space applications. In 1984 the rights to the production and development of SPE electrolysers was purchased by Hamilton Sundstrand, a subsidiary of United Technologies Corporation [1]. Since then much research has been carried out on SPE electrolysers and today several commercial SPE electrolysers are in operation. The focus of the research has been on the following aspects:

- Reducing cost by developing cheaper, more active and stable catalysts that will facilitate lower catalyst loadings
- Developing suitable and cost effective membranes
- Improving performances by developing MEAs with lower resistivity between the catalyst layers, membrane and gas diffusion layers
- Improving service life by developing MEAs that have good contact between catalyst layers and the membrane
- Up-scaling SPE electrolyser technology for commercial applications.

Research carried out by various groups with particular emphasis on the development of catalysts for SPE electrolyser anodes is described in this section.

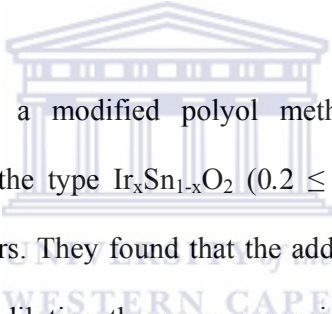
The use of noble metal oxides as catalysts is well established in many industrial electrochemical processes in the form of DSAs, as developed by the Dutch scientist, Henry B. Beer [17, 18]. There are many methods available for the synthesis of noble metal oxides. Most DSA electrodes are prepared by thermal decomposition of the

metal precursors onto a titanium substrate. However, this method is considered to be unsuitable for SPE electrolyzers because of the difficulty in achieving good contact between the catalytic layer and the membrane [18]. Electrodes should also be porous to allow the evolved gases to escape through the layer and therefore the DSA approach is not suitable [44]. To obtain good contact between the catalytic powders and the membrane the catalyst powder can be applied as a catalytic ink to the membrane or synthesized directly onto the surface of, or within, the membrane [18]. Spraying the catalyst particles as a catalytic ink permits the preparation of very large particles using a wide range of techniques [44]. The Adams fusion method, which is the fusion of catalyst precursors with  $\text{NaNO}_3$ , has been widely used to prepare fine noble metal oxide powders. The Adams fusion method has the advantage that the process can be carried out in air at temperatures higher than  $300\text{ }^\circ\text{C}$  for short time periods to afford nanosized metal oxides [45]. The sol-gel method is also useful for preparing noble metal oxides, however, the precursor type as well as the solvent removal stage can affect properties of the produced metal oxides. The polyol method is also a relatively simple method that can be used to prepare nanosized metallic colloids of iridium and ruthenium, which can then be oxidized in air to afford the corresponding metal oxides. The polyol method involves the reduction of catalyst precursors in ethylene glycol [18].

Rasten [1], during the research he carried out for his Doktor Ingeniør degree, developed and optimized catalysts for the SPE water electrolyzer. He obtained a cell voltage of  $1.59\text{ V}$  at practical operating conditions of the electrolyzer,  $1\text{ A cm}^{-2}$  and  $90\text{ }^\circ\text{C}$ , using an  $\text{Ir}_{0.7}\text{Ru}_{0.3}\text{O}_2$  anode and a catalyst loading of  $2.4\text{ mg cm}^{-2}$ . Electrical conductivity was found to be the most important limitation of the SPE electrolyzer



due to the porous backing/current collector system which increased the length of the current path and provided a narrower cross-section for electron transport. He developed anode catalysts with different properties and found that the mixed oxide of Ir-Ta (85 mol % Ir) exhibited the highest voltage efficiency at a current density of 1 A cm<sup>-2</sup>. The mixed oxide of Ir-Ru (60–80 mol % Ir) exhibited the highest voltage efficiency for current densities above 1 A cm<sup>-2</sup>. Pt black was found to be more suitable as cathode catalyst than Pt on carbon since the carbon particles introduced an unnecessary porosity into the catalytic layer resulting in a high ohmic drop. RuO<sub>2</sub> did not perform well as a cathode catalyst due to insufficient electrochemical activity and too low electrical conductivity.



Marshall *et al.* [46] used a modified polyol method for the preparation of nanocrystalline powders of the type Ir<sub>x</sub>Sn<sub>1-x</sub>O<sub>2</sub> (0.2 ≤ x ≤ 1) as oxygen evolution catalysts for SPE electrolyzers. They found that the addition of SnO<sub>2</sub> to IrO<sub>2</sub> had no beneficial effect other than diluting the more expensive IrO<sub>2</sub>. Cyclic voltammetry (CV) results revealed that the number of active sites decreased as the tin content increased. They also found that the addition of up to 20% tin was acceptable; little change in the active area was observed for low tin content. However, at low tin content there was still a 40 mV increase in cell voltage at 1 A cm<sup>-2</sup> at 80 °C. The group recorded the best results with pure IrO<sub>2</sub> when using a cell voltage of 1.61 V at 1 A cm<sup>-2</sup> at 90 °C.

Slavcheva *et al.* [47] investigated the use of reactive magnetron sputtering for the deposition of thin films of IrO<sub>2</sub> as catalyst for the PEM electrolyser. The sputtered films possessed excellent mechanical stability and corrosion resistance at high anodic

potentials where oxygen evolution takes place. They obtained the best performance with a 500 nm thick film containing  $0.2 \text{ mg cm}^{-2}$  catalyst at an anodic current density of  $0.3 \text{ A cm}^{-2}$  at 1.55 V (versus RHE). They concluded that the dc magnetron sputtering in argon/oxygen plasma was a reliable method for catalyst deposition because reproducible homogeneous films with controllable thickness and extended microporous structure could be obtained.

Marshall *et al.* [25] investigated the use of various binary and ternary metal oxides, using  $\text{IrO}_2$  as the base material. They prepared the electrode by spraying the catalytic powders onto a titanium substrate and then carried out CV and steady-state polarization measurements. The best result was obtained with an  $\text{Ir}_{0.6}\text{Ru}_{0.4}\text{O}_2$  anode and a 20 wt % Pt/C cathode, using Nafion 115 as polymer electrolyte: 1.567 V at  $1 \text{ A cm}^{-2}$  at  $80 \text{ }^\circ\text{C}$ . This equated to a cell efficiency of 94.4% and an energy consumption of  $3.75 \text{ kWh Nm}^{-3} \text{ H}_2$  at  $1 \text{ A cm}^{-2}$ . For the Ir-Ru oxides they found the maximum to be 40 mol % Ru, whereas for the ternary system  $\text{Ir}_x\text{Ru}_y\text{Ta}_z\text{O}_2$  they found the maximum to be about 20 mol % Ru. The lower charge for the electrodes containing high levels of ruthenium is due to the effect that it has on the oxide crystallinity. X-ray photoelectron spectroscopy (XPS) and extended X-ray absorption fine structure analysis showed that increasing the ruthenium content resulted in more ordered oxide structures, which presumably were less rough and had fewer defects. Since tantalum does not directly take part in the charging process the total charge decreased as the tantalum content increased. The catalytic activity increased almost linearly with ruthenium content and tantalum had no effect on the specific activity of the material. The group also concluded, based on steady state polarization analysis, that the active surface area was not solely responsible for the catalytic activity of these oxides. The

type of noble metal used had an effect on the specific electrochemical activity, which is a property unaffected by surface area.

Ma *et al.* [48] prepared an iridium catalyst supported on nanosized titanium carbide (TiC) as catalyst for the PEM water electrolyser. The Ir/TiC catalyst was prepared by chemical reduction and deposition via ultrasonic dispersion. The iridium particles deposited on TiC had diameters of 10–40 nm. The Ir/TiC catalyst had a pore volume of  $0.1425 \text{ cm}^3 \text{ g}^{-1}$ , which is about twice that of unsupported Ir black catalyst. SEM, TEM, XRD and EDS analyses revealed that the iridium particles were nearly uniformly deposited on the TiC surface and exhibited fine variable crystallites and crystal lattice defects, which increased the density of the active sites and in turn greatly improved the catalytic activity of the Ir/TiC catalyst. CV revealed that the peak current density at 1.5 V (versus a saturated calomel electrode, SCE) on the Ir/TiC catalyst was about 9 times that of the unsupported Ir black catalyst and potentiostatic analysis revealed that the charge passed by the Ir/TiC catalyst after 10 minutes at 1.3 V was about 15 times that of the unsupported Ir black catalyst. The group concluded that the Ir/TiC catalyst was chemically and electrochemically stable under a wide range of experimental potentials and that the catalytic activity of Ir/TiC towards the OER was significantly higher than that of the unsupported Ir black catalyst.

Cheng *et al.* [49] used the Adams fusion method to prepare catalysts with the general formula  $\text{Ir}_x\text{Ru}_{1-x}\text{O}_2$  for the SPE electrolyser. The  $\text{Ir}_x\text{Ru}_{1-x}\text{O}_2$  ( $x = 0.2, 0.4, 0.6$ ) compounds were found to be more active than pure  $\text{IrO}_2$  and more stable than pure  $\text{RuO}_2$ . The catalytic activity increased as the ruthenium content increased. CV

revealed that  $\text{Ir}_{0.2}\text{Ru}_{0.8}\text{O}_2$  had the most active sites. An  $\text{Ir}_{0.2}\text{Ru}_{0.8}\text{O}_2$  anode with 1.7 mg  $\text{cm}^{-2}$  noble metal loading, and a 24.8% Pt/C cathode, had a cell performance of 1.622 V at 1 A  $\text{cm}^{-2}$  and 80 °C.

The GenHyPEM [15] project commenced in October 2005 with the goal to develop a low cost high pressure (50 bar) PEM water electrolyser that could produce up to several  $\text{Nm}^3 \text{H}_2/\text{h}$ . Thus far, non-noble catalysts to replace platinum in the HER have been identified and stable performances under high operating current densities (1 A  $\text{cm}^{-2}$ ) have been obtained. This already paves the way for substantial cost reductions. Stack efficiencies of up to 65% with 1  $\text{Nm}^3 \text{H}_2/\text{h}$  capacity electrolysers operating at high (1 A  $\text{cm}^{-2}$ ) current densities have also been achieved. It has been found that hydrogen can be safely produced in the 1–10 bar pressure range, offering the possibility of direct storage in hydride tanks at moderate pressures. Optimized electrolysers with up to 5  $\text{Nm}^3 \text{H}_2/\text{h}$  output capabilities have also been developed within the GenHyPEM consortium by industrial partners and some are commercially available for various industrial applications.

## **2.2 Metal oxides as anode catalysts for solid polymer electrolyte electrolysers**

### **2.2.1 $\text{IrO}_2$ as anode catalyst**

$\text{IrO}_2$  has a wide range of applications, such as electrodes in electrochromic devices, oxygen barriers in advanced memory technology, solar cell electrolytic systems, optical disc storage memory, pH sensors, electrodes for neural stimulation and catalysts for water electrolysers [50]. The use of  $\text{IrO}_2$  as catalyst for oxygen evolution has attracted the attention of many scientists over recent years.  $\text{IrO}_2$  as a catalyst exhibits high corrosion resistance and shows only slightly inferior activity compared

to RuO<sub>2</sub> [38]. IrO<sub>2</sub> offers a lower anodic overpotential (100 mV at 1 A cm<sup>-2</sup>) and long term stability. IrO<sub>2</sub> also show less efficiency loss due to corrosion or poisoning [48]. IrO<sub>2</sub> is however very expensive. This has led to research being carried out into composite materials with the aim of reducing the quantity of IrO<sub>2</sub> required, without appreciable loss of catalytic activity and with possible improvement in anodic stability [51].

### **2.2.2 Ir-Sn mixed oxides as anode catalysts**

SnO<sub>2</sub> is an n-type broad-band gap (3.6 eV) oxide semiconductor with high chemical and mechanical stabilities. SnO<sub>2</sub> is a versatile material and is widely used as the most attractive material for gas sensor applications, as catalyst during the oxidation of organic compounds, as key component in rechargeable lithium batteries and a master component in optoelectronic devices [45]. SnO<sub>2</sub> has a rutile structure and has naturally occurring growth faces (110), (101) (which is equivalent to the (011) face) and (100) (equivalent to the (010) face) [52]. It has been suggested that the addition of SnO<sub>2</sub> does not reduce the activity of RuO<sub>2</sub> as much as TiO<sub>2</sub> does [11, 44].

Marshall *et al.* [25] found that when tin is added to iridium (Ir<sub>x</sub>Sn<sub>1-x</sub>O<sub>2</sub>) the active surface area is proportional to the iridium content of the oxide. This is because the tin present in the oxide lattice does not contribute to the charging reaction. They considered tin additions (up to 20–30 mol %) to be reasonable as the total area only decreased by 10–15%, which probably resulted in an overall cost benefit considering the cost of iridium and tin. The crystal properties of Ir<sub>x</sub>Sn<sub>1-x</sub>O<sub>2</sub> powders depend on the synthesis method used to prepare the materials. Use of the Adams fusion method results in an oxide having at least two separate oxide phases, with one of the phases

containing mostly SnO<sub>2</sub>. The modified polyol method was believed to result in the formation of a solid solution between IrO<sub>2</sub> and SnO<sub>2</sub>, with the lattice parameters increasing linearly with tin content. The addition of tin led to an increase in the average crystal size from about 3.5 to 15nm [18].

De Pauli and Trasatti [51] prepared IrO<sub>2</sub>-SnO<sub>2</sub> mixed oxides via a thermal decomposition method at 400 °C. XPS and CV showed that the surface of the mixed oxides was considerably rich in IrO<sub>2</sub>. For IrO<sub>2</sub> contents > 10 mol %, the IrO<sub>2</sub>-SnO<sub>2</sub> mixed oxide electrodes behaved as pure IrO<sub>2</sub>. At IrO<sub>2</sub> contents < 40 mol % the activity for unit surface charge (at constant surface concentration of IrO<sub>2</sub>) decreased with decreasing IrO<sub>2</sub> content. The surface structure and composition of the mixed oxide electrodes was stable under high oxygen evolution.

### **2.2.3 Ir-Ru mixed oxides as anode catalysts**

Mixed ruthenium based oxides have been studied since the late 1950s, when it was discovered that these materials possess favourable catalytic properties [11]. RuO<sub>2</sub> is known to be the most active towards the OER but suffers from instability, and should thus be stabilized with another metal oxide such as IrO<sub>2</sub> or SnO<sub>2</sub> [25, 44]. In practice it was found that RuO<sub>2</sub> possesses considerable stability due to sufficient electronic conductivity in the oxide, which prevents the reduction of the oxide. The addition of the second metal oxide thus serves to stabilize, as well as increase, the catalytic activity of RuO<sub>2</sub> [11, 44]. For Ir-Ru oxides it is said that a maximum in anodic charge is often found at intermediate compositions [25, 44].

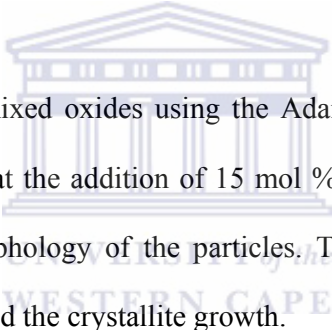
Marshall *et al.* [25] found that, based on XRD and XPS results, the reduction in active surface area can be explained by the decrease in the concentration of noble metal elements at the surface of the particles. This was largely due to the synthesis of the oxide in which ruthenium components strongly cluster together, resulting in a heterogeneous particle structure, where the active ruthenium component is found predominantly in the inner core of the particle. However since most electrochemical processes occur at the surface, the ruthenium-rich core does not play a role in the charging reaction.

Cheng *et al.* [49] observed a single rutile-like phase in the XRD spectra of  $\text{Ir}_x\text{Ru}_{1-x}\text{O}_2$ . They found that as the ruthenium content increased, the average particle size of the catalyst also increased. Their research concluded that the addition of as low as 20 mol %  $\text{IrO}_2$  can improve the stability of  $\text{RuO}_2$  and that at 40 mol %  $\text{IrO}_2$ , they observed considerable stability of  $\text{Ir}_{0.4}\text{Ru}_{0.6}\text{O}_2$  at  $0.5 \text{ A cm}^{-2}$  and  $80 \text{ }^\circ\text{C}$  testing in a single cell for 100 hours.

Ma *et al.* [53] studied the effect of calcining temperature on  $\text{RuO}_2$  as anode catalyst for the PEM electrolyser. They prepared the  $\text{RuO}_2$  using the Adams fusion method, which involved a pyrolysis process in a nitrate melt at  $300 \text{ }^\circ\text{C}$  followed by calcining at temperatures ranging from  $350$  to  $550 \text{ }^\circ\text{C}$ . Electrochemical impedance spectroscopy (EIS) results clearly showed that the catalytic activity of  $\text{RuO}_2$  decreased with increasing calcining temperature. They also observed an increase in particle size of  $\text{RuO}_2$ , an increase in the crystallinity of the material, and that the conductivity of the material increased as the calcining temperature increased. The optimum calcining temperature for  $\text{RuO}_2$  was found to be  $350 \text{ }^\circ\text{C}$ .

### 2.2.4 Ir-Ta mixed oxides as anode catalysts

Ir-Ta oxides have high activity and corrosion stability. It has been suggested that they are the most efficient catalysts for the OER in acidic media [25]. The IrO<sub>2</sub>-Ta<sub>2</sub>O<sub>5</sub> system as DSAs is a promising catalyst in various electrochemical industries, such as cleaning of waste water and electrowinning (electroextraction) of metals, where oxygen evolution is the main anodic reaction. Ta<sub>2</sub>O<sub>5</sub> is mainly added to improve the service life of IrO<sub>2</sub>, which is the active catalyst and the most expensive component [1]. IrO<sub>2</sub>-Ta<sub>2</sub>O<sub>5</sub> with the composition 70% IrO<sub>2</sub> and 30% Ta<sub>2</sub>O<sub>5</sub> has been verified to be the best combination in binary oxide systems in present commercial applications [54].



Rasten [1] prepared Ir-Ta mixed oxides using the Adams fusion method and, from TEM images, determined that the addition of 15 mol % Ta had a great influence on the crystallite size and morphology of the particles. Ta<sub>2</sub>O<sub>5</sub> enriched the crystallite surface of IrO<sub>2</sub> and suppressed the crystallite growth.

Hu *et al.* [54] studied the ageing of IrO<sub>2</sub>-Ta<sub>2</sub>O<sub>5</sub> anodes, in H<sub>2</sub>SO<sub>4</sub> solution, over an extended period of electrolysis. They found that the electrolysis processes of these anodes could be divided into three stages, i.e. 'active', 'stable' and 'de-active' stages. During the first two stages dissolution of the coated oxides dominates, with preferential loss of the IrO<sub>2</sub> component. This results in a decrease in current for oxygen evolution and voltammetric charge. They found that in the first two stages the preferential orientations of the 110 and 101 planes in IrO<sub>2</sub> (rutile) decreased with electrolysis time and the 002 plane increased, while the preferential orientations remained stable in the 'de-active' stage. EIS measurements showed a slight increase

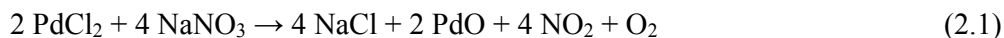


in reaction resistance of the oxide catalysts in the ‘de-active’ stage while a sharp increase in total physical impedance was observed for the whole anode.

### **2.2.5 Ir-Pd mixed oxides as anode catalysts**

Palladium, like other noble metals, exhibits high catalytic activity towards several electrochemical processes, such as the HER, hydrogen absorption and the reduction of simple organic compounds [55]. In many instances palladium is superior to platinum [56]. The main difference between the two is that palladium has the unique ability to absorb hydrogen, under both gas-phase and electrochemical conditions. The electrochemical hydrogen absorption into palladium occurs in the potential range where the UPD of hydrogen takes place as well as in the range of the HER [55].

Shriner and Adams [56] successfully prepared platinum oxides by fusion with NaNO<sub>3</sub> and also used this method to prepare palladium oxides. There are three known oxides of palladium corresponding to the formulae PdO, PdO<sub>2</sub> and Pd<sub>2</sub>O<sub>3</sub>, and their hydrates. Most palladium oxides are not stable, especially in water. PdO<sub>2</sub> decomposes at ambient temperatures into PdO and O<sub>2</sub>. The reaction that takes when preparing palladium oxide is illustrated by equation 2.1:



If PdO<sub>2</sub> forms during the reaction it will be immediately decomposed by either the high temperature or later treatment with water. They found that palladium oxide is most active when the fusion temperature is 600 °C and that it is an effective catalyst for hydrogenation.

### 2.3 Conclusion

Information and data from various research groups was obtained. The different groups used several different methods to prepare the catalysts and MEAs, different catalyst loadings and different types of metals/metal oxides as catalysts. Marshall *et al.* obtained a cell voltage of 1.567 V at 1 A cm<sup>-2</sup> and 80 °C when using an Ir<sub>0.6</sub>-Ru<sub>0.4</sub>O<sub>2</sub> anode, 20 wt % Pt/C cathode and a Nafion 115 membrane [25]. Rasten also achieved the best cell performance with an Ir<sub>0.7</sub>Ru<sub>0.3</sub>O<sub>2</sub> anode, namely a cell potential of 1.59 V at 10 kA m<sup>-2</sup> at 90 °C [1]. These results indicate that the IrO<sub>2</sub>-RuO<sub>2</sub> mixed oxides are promising as anode catalysts for SPE electrolyzers for industrial applications. For pure IrO<sub>2</sub> a cell potential of 1.61 V at 1 A cm<sup>-2</sup> and 90 °C was obtained [46].

Binary metal oxides have been clearly identified to have higher activity and greater stability than IrO<sub>2</sub> or RuO<sub>2</sub>. However, the addition of SnO<sub>2</sub> to IrO<sub>2</sub> has proved only to dilute the expensive IrO<sub>2</sub>, with no further beneficial effects [46]. IrO<sub>2</sub>-Ta<sub>2</sub>O<sub>5</sub> with the composition of 70% IrO<sub>2</sub> and 30% Ta<sub>2</sub>O<sub>5</sub> has been verified to be the best combination in binary oxide systems in present commercial applications [54]. The addition of RuO<sub>2</sub> to IrO<sub>2</sub> has resulted in significant improvements in cell performances, as can be concluded from the work done by the various research groups. RuO<sub>2</sub> serves to improve the catalytic activity of IrO<sub>2</sub> and IrO<sub>2</sub> improves the stability of RuO<sub>2</sub> [44, 49]. Shriner and Adams have shown that the Adams fusion method is suitable for the preparation of palladium oxides [56]. Very few groups have studied binary metal oxides based on Ir-Pd as anode catalysts for SPE electrolyzers. No information on these oxides was available in the open literature at the time of this research study. Platinum is the preferred cathode catalyst in SPE electrolyser technology due to its high stability and high electrochemical activity towards the HER [1].

The main conclusions of this literature review are the following:

- The anode catalyst activity and stability is crucial for further development of the SPE electrolyser.
- The catalyst preparation method and the conditions used have a significant impact on the activity of the catalysts.
- IrO<sub>2</sub>-RuO<sub>2</sub> and IrO<sub>2</sub>-TaO<sub>5</sub> systems are the most promising anode catalysts towards the OER, in industrial applications.
- Ir-Pd mixed oxides might be suitable as anode catalysts.



## Chapter 3: Experimental

### 3.1 Chemicals and apparatus

Chemicals used for the preparation of the metal oxide catalysts and the preparation of the anodes are given in Tables 3.1 and 3.2, respectively.

**Table 3.1 Chemicals used for metal oxide catalyst preparation.**

Chemical	Supplier
H <sub>2</sub> IrCl <sub>6</sub>	SA Precious Metals
RuCl <sub>3</sub>	SA Precious Metals
SnCl <sub>2</sub> .2H <sub>2</sub> O	John Matthey, Alfa-Aesar
TaCl <sub>5</sub> (99.995%)	John Matthey, Alfa-Aesar
PdCl <sub>2</sub>	John Matthey, Alfa-Aesar
NaNO <sub>3</sub>	Holpro Analytical
Isopropanol	John Matthey, Alfa-Aesar

**Table 3.2 Chemicals used for anode preparation.**

Chemical	Supplier
Titanium mesh	Bekinit KK
Oxalic acid	NT Laboratory Supplies
Nafion solution 5 wt %	Aldrich
Isopropanol	John Matthey, Alfa-Aesar

All water was tapped from a Milli-Q<sup>®</sup> ultrapure water system. The resistance of the water was 18.3 MΩ.cm.

Equipment: Potentiostat: PGSTAT20, Echo Chemie

Muffle furnace with electrical heating: Kiln Contracts

Airgun: Badger<sup>™</sup> (100-LGF)

Oven with electrical heating: Labcon

Ultrasonic bath: Integral Systems

Centrifuge: Sigma.

### **3.2 Metal oxide preparation**

The Adams fusion method, first described by R. Adams and R.L. Shriner [57], entails the fusion of the metal chloride precursor with sodium nitrate in air at elevated temperatures. The method has since been used to prepare various noble metal oxides [1, 25, 49, 56, 57]. A fully detailed description of the method is however not reported in the literature and thus various groups have modified the method in order to obtain the respective desired results. In this study a predetermined quantity of the catalyst precursor was dissolved in 10 ml isopropanol until a metal concentration of  $3.5 \times 10^{-2}$  M was achieved and magnetically stirred for 1.5 hours. Five grams of finely ground  $\text{NaNO}_3$  was added to the solution, which was then further stirred for 30 minutes. The mixture was then placed in a preheated oven (at  $80^\circ\text{C}$ ) for 30 minutes, until all the isopropanol had evaporated. The dried catalyst precursor/salt mixture was then fused in a preheated furnace (from  $250$  to  $500^\circ\text{C}$ ). The obtained metal oxide was then cooled and washed with ultrapure water until all the unreacted  $\text{NaNO}_3$  was removed. The final step was to dry the metal oxide in an oven at  $100^\circ\text{C}$ .

#### **3.2.1 Optimization of the preparation conditions of $\text{IrO}_2$**

In order to achieve the most active  $\text{IrO}_2$  catalyst the preparation conditions, specifically reaction time and temperature, were optimized. First, the temperature of  $500^\circ\text{C}$  was chosen (based on the literature) and the reaction time was varied from 0.5 to 4 hours. The best reaction time obtained was then kept constant while varying the fusion temperature from  $250$  to  $500^\circ\text{C}$ . The best preparation conditions (reaction time and temperature) to prepare the in-house  $\text{IrO}_2$  catalyst were then applied to prepare

the binary metal oxide catalysts. The term in-house refers to the catalysts synthesized adapting the Adams fusion method.

### **3.2.2 Preparation of binary metal oxides**

Optimization of the reaction time and temperature for the preparation of the binary metal oxides was not carried out because of time constraints. All binary metal oxides were prepared via the Adams fusion method by applying the best preparation conditions obtained for the preparation of the in-house IrO<sub>2</sub> catalyst. Only the compositions of the binary metal oxides were optimized. Iridium was used as the base material for all binary metal oxides. For each type of binary metal oxide system the second metal (Sn, Ru, Ta or Pd) was added in a concentration of 5–30 mol % to iridium.

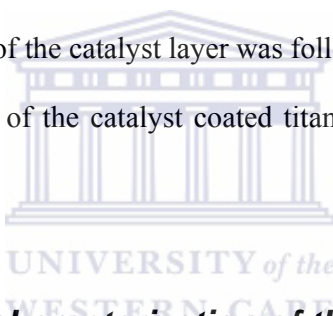
## **3.3 Preparation of the working electrode (anode)**

### **3.3.1 Glassy carbon working electrode**

A glassy carbon working electrode was used for electrochemical measurements to determine the most active IrO<sub>2</sub> catalyst (optimization). The area of the glassy carbon electrode was 0.196 cm<sup>2</sup>. Catalyst ink was prepared by mixing together the prepared metal oxide, Nafion solution (5 wt %) and ultrapure water (ratio 1:6:2). The mixture was then ultrasonically dispersed for 15 minutes. A carefully measured drop of the catalyst ink was deposited using a micropipette onto the thoroughly cleaned glassy carbon surface. Catalyst loading equated to 0.61 mg cm<sup>-2</sup>.

### **3.3.2 Catalyst coated titanium mesh working electrode**

The activities of all binary metal oxide catalysts as well as the commercial and best in-house IrO<sub>2</sub> catalyst were tested using a catalyst coated titanium mesh working electrode. A predetermined size of titanium mesh was cut and boiled in oxalic acid for 12 minutes to remove surface oxides. Catalyst inks were prepared by mixing together the prepared metal oxides, Nafion solution (5 wt %) and ultrapure water (ratio 1:6:2). A measured volume of isopropanol was added to serve as dispersion medium. The mixture was then ultrasonically dispersed for 30 minutes. An airbrush was used to spray the catalyst ink (1 mg cm<sup>-2</sup>) onto the pretreated titanium mesh. The catalyst ink was thoroughly dried between each layer sprayed to prevent agglomeration of the catalytic particles. Spraying of the catalyst layer was followed by spraying of a Nafion layer (1 mg cm<sup>-2</sup>). The area of the catalyst coated titanium mesh working electrode was 0.785 cm<sup>2</sup>.



## **3.4 Electrochemical characterization of the catalysts**

### **3.4.1 Electrochemical cell setup**

A standard three-electrode cell was used for all the electrochemical characterizations. A glassy carbon electrode or the titanium mesh electrode, as described earlier, was used as the working electrode. A 3 M Ag/AgCl reference electrode that has a +0.210 V shift (compared to a standard hydrogen electrode, SHE) was used. All the potentials reported in this study are relative to the SHE. A platinum mesh counter electrode was used. A 0.5 M H<sub>2</sub>SO<sub>4</sub> solution was used as the electrolyte for all electrochemical measurements.

### **3.4.2 Electrochemical measurements**

Autolab potentiostat PGSTAT20 (Eco-Chemie) was used for electrochemical characterization. The activity and stability (short term stability for 30 minutes) of the metal oxides were studied by applying a fixed potential (V) and measuring the current (mA) response. Potentials of up to 1.8 V were applied and the catalytic response of the oxides determined.

## **3.5 Physiochemical characterization of the catalysts**

### **3.5.1 Scanning electron microscopy**

SEM was used to study the surface morphology of the catalysts. SEM imaging was carried out on a Hitachi X-650 SEM using GENESIS software. Energy dispersive spectroscopy (EDS) was also carried out using this equipment to study the composition and distribution of the metal components.

Operating parameters used for SEM analysis were the following:

Working distance: 15 mm

Accelerating gun filament: Tungsten

Accelerating voltage: 25 KeV

Filament current: 75–80  $\mu$ A

Magnification: 5000x

### **3.5.2 Transmission electron microscopy**

When dealing with nanoparticles it is important to be able to determine the aggregation state, particle size and morphology. The homogeneity of particle size or shape on the atomic scale is important as it relates to the physical properties of nanosized materials. TEM is an indispensable technique for the study of metal nanoparticles. High-resolution transmission electron microscopy not only provides



information on particle size and shape but also on the crystallography of monometallic and bimetallic nanoparticles [58]. In this study TEM was exclusively used to study the particle size and dispersion of the catalysts. Selected area electron diffraction analysis was not carried out but XRD analysis was performed to study the crystallographic nature of the catalysts. TEM images of catalysts were recorded using a Tecnai G<sup>2</sup> F20 X-Twin Mat200 kV Field Emission TEM.

Experimental parameters used for TEM analysis were the following:

Accelerating voltage: 200 kV

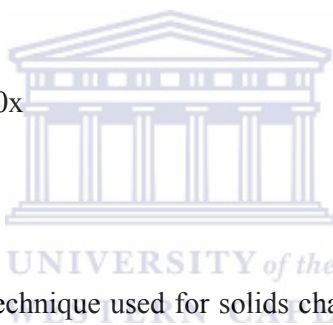
Current: 20 mA

Condenser aperture: 1

Objective aperture: 3

Exposure time: 3 s

Magnification: 88 000x



### 3.5.3 X-ray diffraction

XRD is the most powerful technique used for solids characterization. The diffraction pattern used permits both qualitative and quantitative crystal structure analysis, as well as crystallite size and distribution determination. In this study XRD was used specifically to determine the crystal structure and particle size of the catalysts. The Scherrer formula (equation 3.1) was used to determine the average particle sizes of the catalysts

$$D = 0.9\lambda / \beta \cos \theta \quad (3.1)$$

where D is the particle size, 0.9 is the shape factor,  $\lambda$  is the X-ray wavelength,  $\beta$  is the peak width at half peak height (radians), and  $\theta$  is the angle of reflection.

Experimental parameters used for XRD analysis were the following:

X-ray diffractometer: Bruker AXS D8 Advance

X-ray source: Copper tube with Cu  $K_{\alpha}$  ( $\lambda = 1.5406 \text{ \AA}$ )

X-ray detector: Sodium iodide

Monochromator: Graphite

Generator operation: 40 kV and 40 mA

Electron intensity: 40 kV

Current: 30 mA

Scan range ( $2\theta^{\circ}$ ): 0–90

Scan rate:  $0.05^{\circ} \text{ min}^{-1}$



## Chapter 4: Results and discussion

### 4.1 Optimization of the $\text{IrO}_2$ catalyst

#### 4.1.1 Effect of reaction time on the activity of $\text{IrO}_2$

The preparation conditions play an important role in the behaviour of the metal oxides as catalysts. Thus in order to obtain the most active catalysts it is necessary to optimize the catalyst synthesis method. In this study, the Adams fusion method was adapted and the preparation conditions were optimized for improved catalytic activity. In order to optimize the reaction time, the temperature was kept constant at 500 °C and the reaction time was varied from 0.5 to 4 hours. Chronoamperometry analysis (Figures 4.1 and 4.2) revealed a clear trend in catalytic activity: maximum catalytic activity by the  $\text{IrO}_2$  catalyst was achieved when using a reaction time of 2 hours and a temperature of 500 °C. All potentials reported in this study are relative to a SHE.

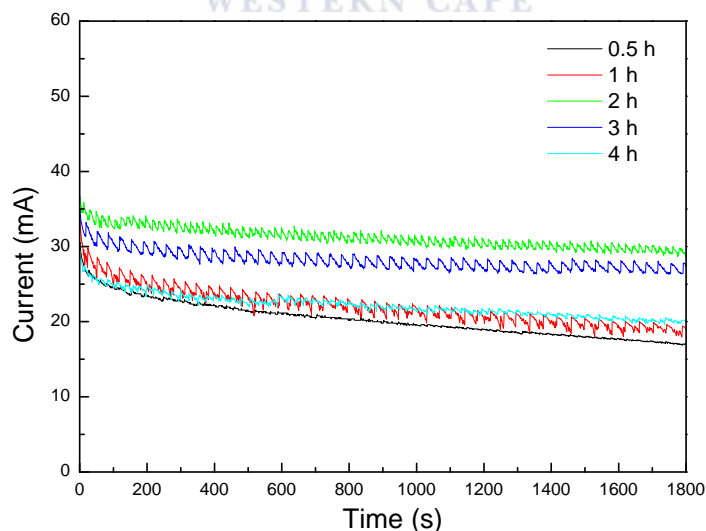
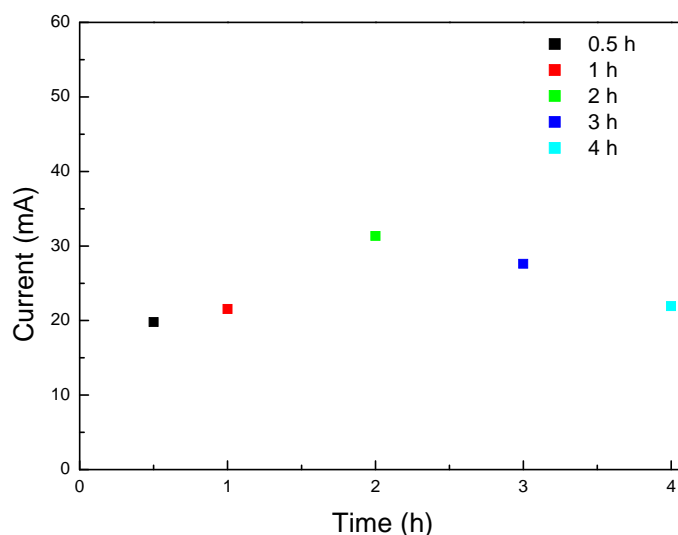


Figure 4.1: Catalytic activity of in-house  $\text{IrO}_2$  at 1.8 V  
(500 °C, 0.5–4 hours).



**Figure 4.2: Peak catalytic activity of in-house IrO<sub>2</sub> at 1.8V**

(500 °C, 0.5–4 hours).

The observed increase in catalytic activity as the reaction time increased from 0.5 to 2 hours was most likely due to the increased availability of the active sites and a high surface area resulting from such a homogeneous dispersion, and an increased number of smaller particles. The decrease in catalytic activity observed for reaction times longer than 2 hours was most likely due to the decreased availability of the active sites caused by the larger particles (revealed by XRD and TEM) rather than a decrease in specific catalytic activity [46].

XRD analysis (Figure 4.3) revealed the presence of a rutile oxide phase, showing the (110) and (101) orientations of IrO<sub>2</sub>, which are both close-packed planes for the iridium atom [54] and is comparable to the standard XRD pattern. XRD analysis revealed an increasing trend in crystallinity as the reaction time increased. The latter effect contributes to the decrease in active surface area of the catalysts [46]. However,

the optimum particle size depends also on the availability and proximity of the active sites, apart from the surface area [25, 46]. Experiments showed that the optimum particle size (5.5 nm) was achieved in the case of the catalysts synthesized using a reaction time of 2 hours. The Scherrer formula was used to calculate the average particle size for IrO<sub>2</sub>. It was found that the particle size increased with the increase in reaction time i.e., the particle size was found to increase from 4.5 nm for the 0.5 hour sample to about 10 nm for the 4 hour sample.

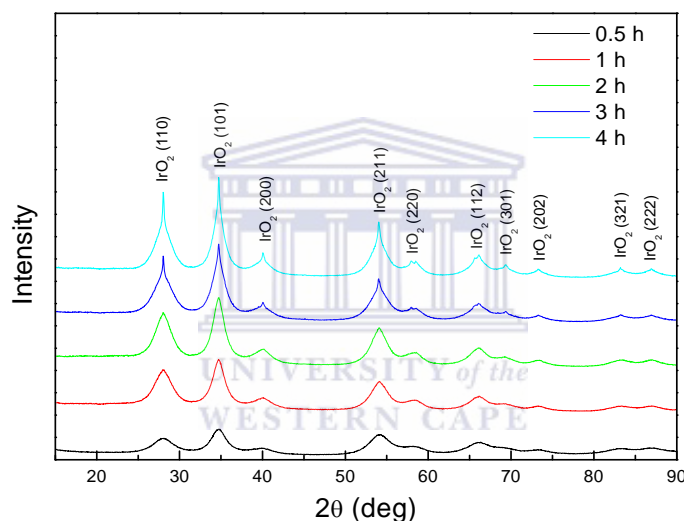
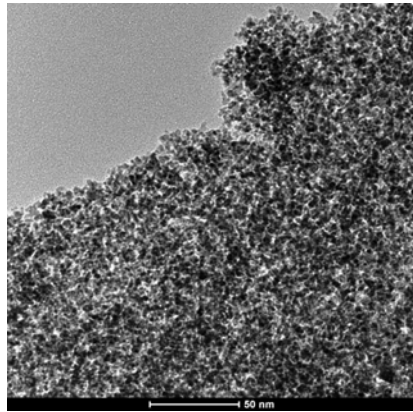


**Figure 4.3: XRD patterns of in-house IrO<sub>2</sub> [59]  
(500 °C, 0.5–4 hours).**

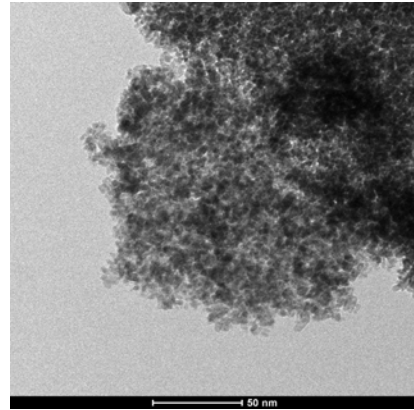
TEM images (Figure 4.4) confirmed the results of XRD analysis, namely that as the reaction time increased the particle size increased. Table 4.1 clearly shows the increase in the particle size with reaction time.

Reaction Time (Hour)	Particle Size (nm)
0.5	4
1	5.5
2	6.5
3	8
4	10

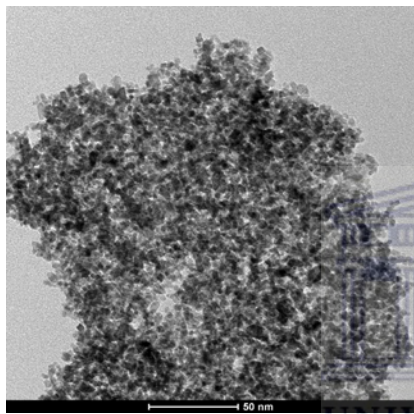
**Table 4.1: Effect of reaction time on the particle size of IrO<sub>2</sub>**



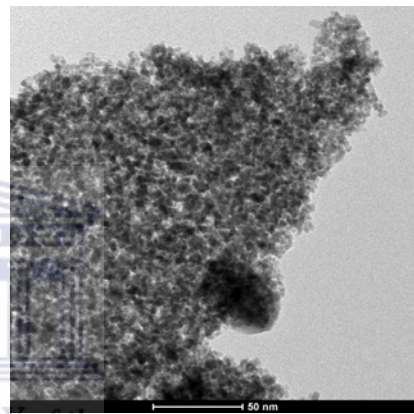
(a) 0.5 hours and 500 °C



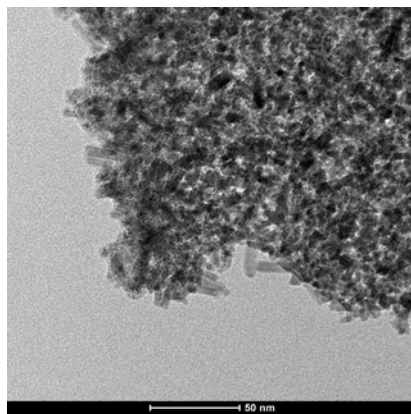
(b) 1 hour and 500 °C



(c) 2 hours and 500 °C



(d) 3 hours and 500 °C



(e) 4 hours and 500 °C

Figure 4.4: TEM images of in-house  $\text{IrO}_2$  (500 °C, 0.5–4 hours).

Scale: 50 nm

Larger needle-like particles were present in the 4 hour sample due to a higher degree of crystallization. SEM images did not show any significant morphological differences between the samples.

#### **4.1.2 Effect of temperature on the activity of IrO<sub>2</sub>**

A reaction time of 2 hours (Section 4.1.1) was found to be best for the preparation of IrO<sub>2</sub>. Therefore during further optimization of the synthesis conditions the reaction time was fixed for 2 hours, and the temperature was varied from 250 to 500 °C. Chronoamperometry (Figures 4.5 and 4.6) revealed a maximum catalytic activity at 1.8 V when IrO<sub>2</sub> was prepared at 350 °C over 2 hours. The interference peaks in Figure 4.5 are due to the formation and release of large oxygen bubbles from the electrode surface. IrO<sub>2</sub> prepared at 350 °C had the highest catalytic activity, which is in line with what is reported in the literature [31]. The decrease in catalytic activity of samples prepared at 450 °C and 500 °C was due to an increase in crystallinity and particle size. The low activity of the catalyst prepared at 250 °C may be due to incomplete decomposition of the iridium precursor to IrO<sub>2</sub>. The unreacted precursors can act as inhibitors by covering the available active sites, or there are simply not enough catalytically active sites available for the reaction to take place.

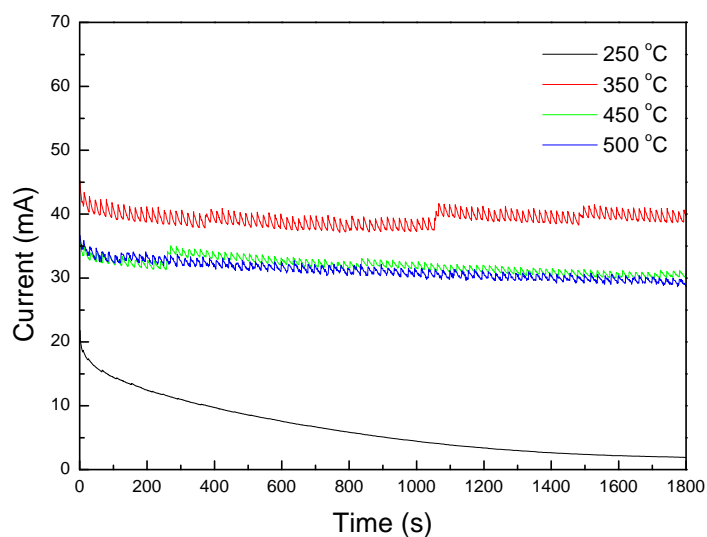


Figure 4.5: Catalytic activity of in-house IrO<sub>2</sub> at 1.8 V

(2 hours, 250–500 °C).

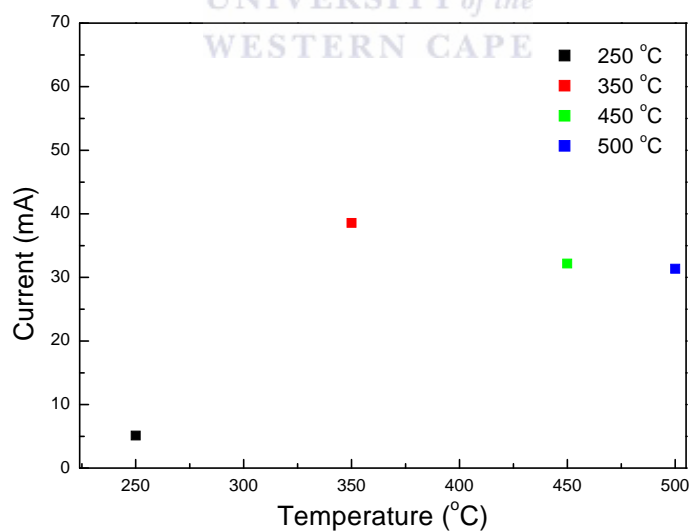
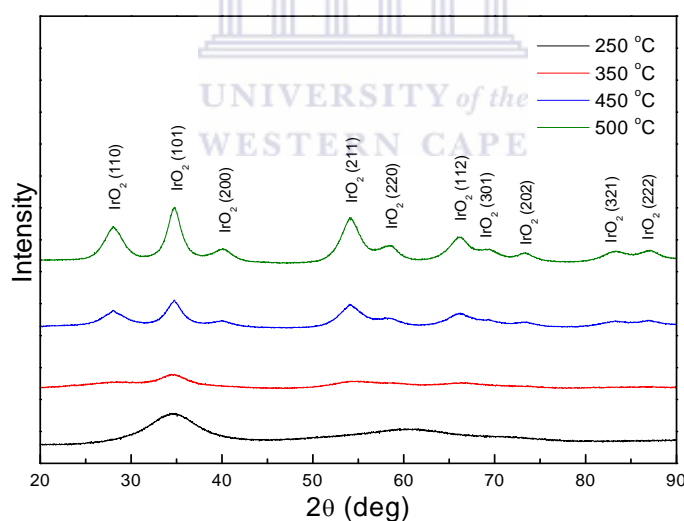


Figure 4.6: Peak catalytic activity of in-house IrO<sub>2</sub> at 1.8V

(2 hours, 250–500 °C).



XRD analysis (Figure 4.7) revealed an increasing trend towards crystallization and a larger particle size as the temperature was increased. IrO<sub>2</sub> prepared at 250–350 °C showed broad peaks, depicting low crystallinity, or the amorphous nature of the particles. It is known that broad amorphous peaks result from smaller particle sizes, which could explain why IrO<sub>2</sub> prepared at 350 °C was most active towards the OER. Rasten *et al.* [31] also found that IrO<sub>2</sub> prepared at 340 °C via the Adams fusion method consisted of nanosized particles with low crystallinity. The average particle sizes of IrO<sub>2</sub> (preparation conditions: 2 hours, 250–500 °C) were calculated using the Scherrer formula. These sizes increased from 1.5 nm for the 250 °C sample to about 5.5 nm for the 500 °C sample. Experiments showed that the optimum particle size (3.5 nm) was achieved in the case of the catalyst synthesized at 350 °C over 2 hours.



**Figure 4.7: XRD patterns of in-house IrO<sub>2</sub> [59]  
(2 hours, 250–500 °C).**

TEM analysis (Figure 4.8) confirmed that the particle size increased with increasing temperature. Table 4.2 clearly shows the increase in the particle size with

temperature. SEM analysis revealed a higher degree of particle agglomeration, resulting in larger particles for IrO<sub>2</sub> prepared at 500 °C over 2 hours.

Temperature (° C)	Particle Size (nm)
250	2.5
350	4.5
450	6
500	6.5

**Table 4.2: Effect of temperature on the particle size of IrO<sub>2</sub>.**

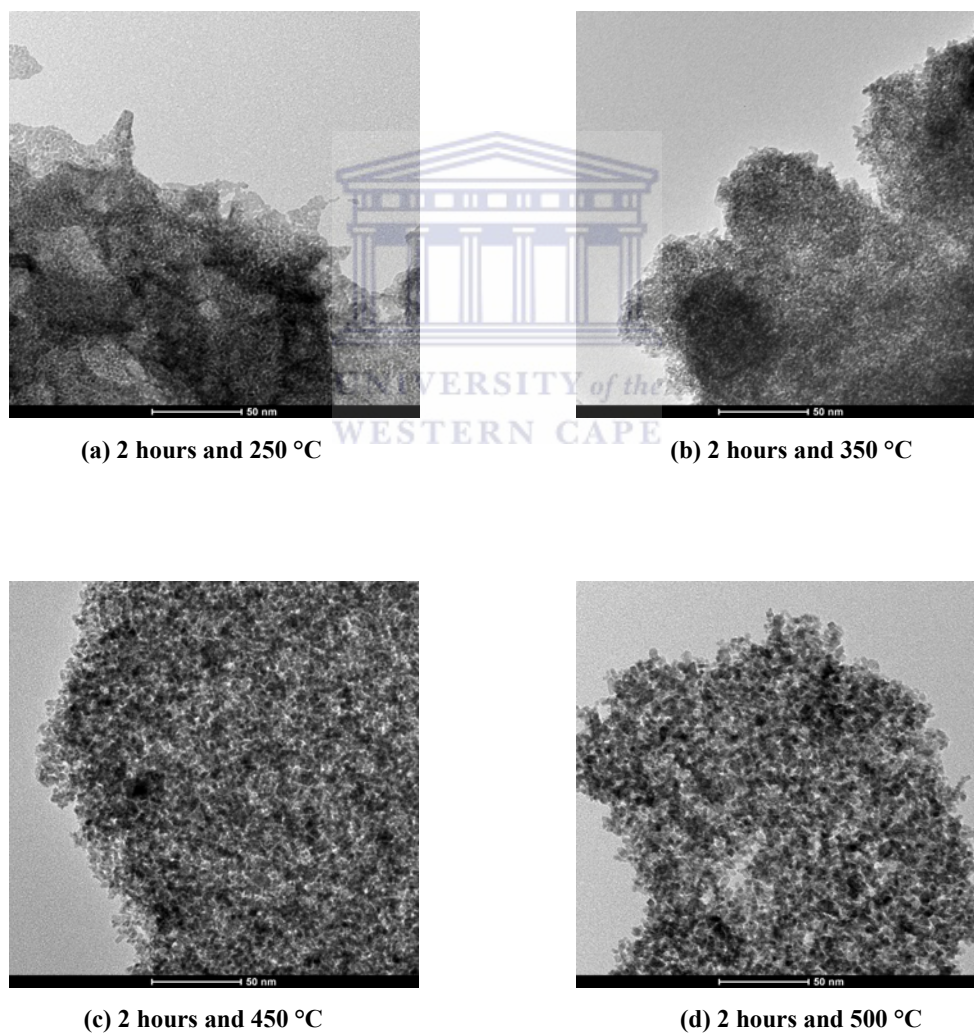


**Figure 4.8: TEM images of in-house IrO<sub>2</sub> (2 hours, 250–500 °C).**

Scale: 50 nm

## 4.2 Comparison of in-house and commercial IrO<sub>2</sub>

Commercial IrO<sub>2</sub> was purchased from Alfa Aesar and used as received for all experiments conducted. Chronoamperometry was carried out using both the glassy carbon and the catalyst coated titanium mesh working electrode. Figure 4.9 shows the catalytic activity of commercial IrO<sub>2</sub> compared to the catalytic activity of the best in-house IrO<sub>2</sub>, at 1.8 V, using the glassy carbon working electrode.

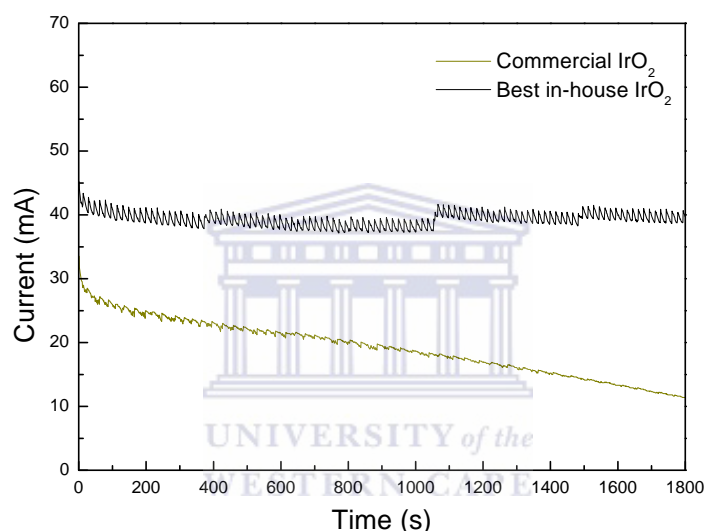


**Figure 4.9: Catalytic activity of commercial and best in-house IrO<sub>2</sub> at 1.8V (glassy carbon working electrode).**

Chronoamperometry revealed that the best in-house IrO<sub>2</sub> had twice the activity of the commercial IrO<sub>2</sub> catalyst. XRD patterns (Figure 4.10) revealed both broad amorphous and sharp crystalline peaks for commercial IrO<sub>2</sub>. XRD data [59] indicated the presence of both metallic iridium and IrO<sub>2</sub> within the commercial IrO<sub>2</sub> sample. Metallic iridium is not known to be beneficial for the OER since the reaction always takes place at an oxide surface [1]. The presence of metallic iridium could be accountable for the low catalytic activity of the commercial IrO<sub>2</sub> catalyst.

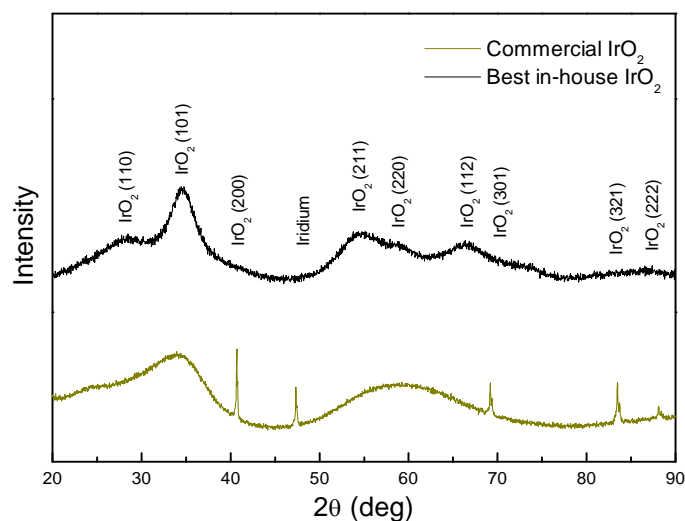
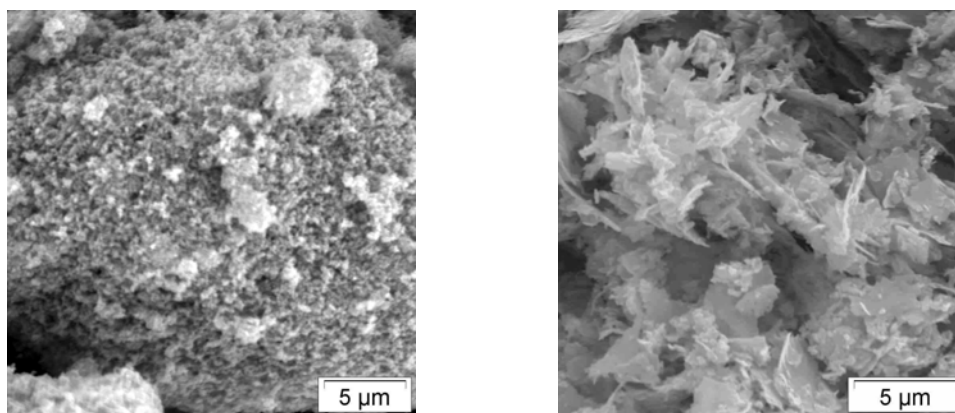


Figure 4.10: XRD patterns of commercial and best in-house IrO<sub>2</sub> [59].

Figures 4.11 and 4.12 show the SEM and TEM images of the commercial and the best in-house IrO<sub>2</sub> catalysts, respectively. SEM revealed a higher degree of particle agglomeration of the commercial IrO<sub>2</sub> catalyst. TEM revealed the presence of particle sizes larger than 50 nm for commercial IrO<sub>2</sub>. The larger particle sizes contributed to the low catalytic activity of commercial IrO<sub>2</sub> because this increased the electronic resistance of the catalyst and decreased the total available active sites.



(a) Commercial IrO<sub>2</sub>

(b) Best in-house IrO<sub>2</sub>

Figure 4.11: SEM images of commercial and best in-house IrO<sub>2</sub>.

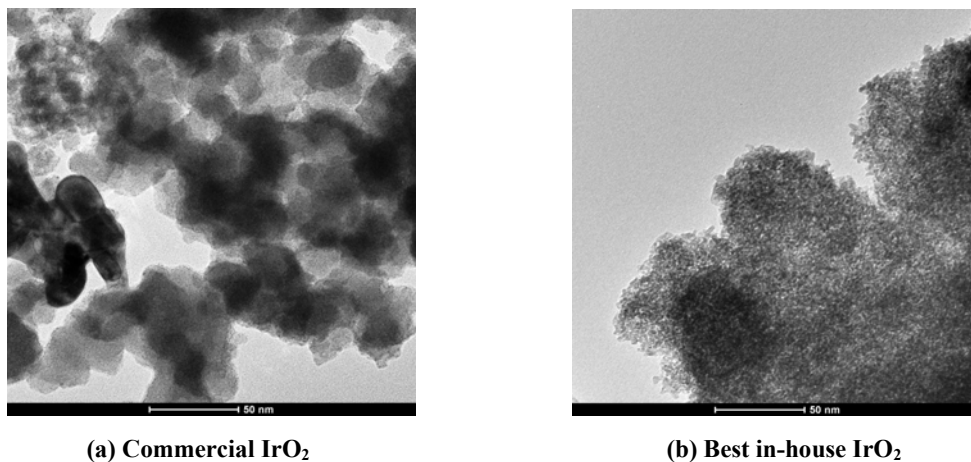


**Figure 4.12: TEM images of commercial and best in-house IrO<sub>2</sub>.**

**Scale: 50 nm**

The use of a titanium mesh as working electrode would resemble more closely the working conditions of the SPE electrolyser than a glassy carbon working electrode (used for the optimization of IrO<sub>2</sub>) due to the gas diffusion properties and the surface conditions of the titanium mesh. Details on the preparation of the working electrodes and the cell setup are discussed in Sections 3.3 and 3.4. The catalyst coated titanium mesh working electrode was therefore adapted and was used to compare the activity of the commercial and best in-house IrO<sub>2</sub> catalysts. Results are shown in Figure 4.13.

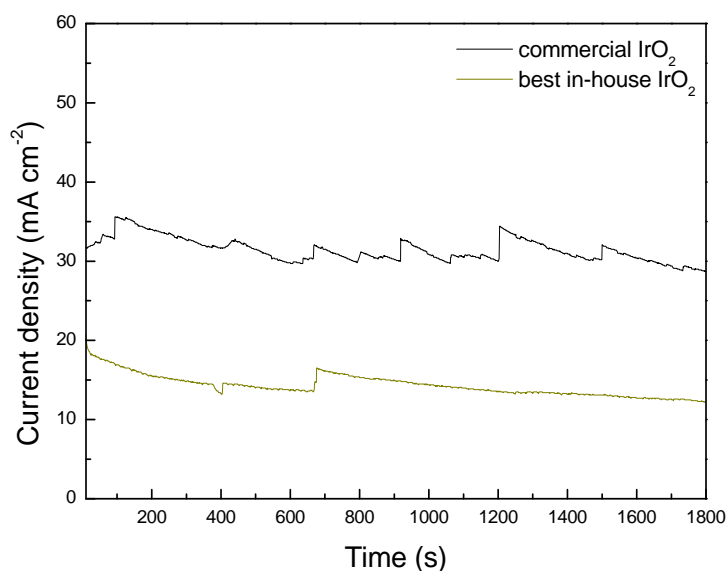


**Figure 4.13: Catalytic activity of commercial and best in-house IrO<sub>2</sub> at 1.8V (catalyst coated titanium mesh working electrode).**

Chronoamperometry revealed that the best in-house IrO<sub>2</sub> had twice the activity of the commercial IrO<sub>2</sub> catalyst. Upon comparing the two working electrodes, both showed that the activity of the best in-house IrO<sub>2</sub> was twice that of the commercial IrO<sub>2</sub> catalyst. This result indicated therefore that the use of the catalyst coated titanium mesh working electrode was a better option for use as a working electrode.

For (the results and discussion of) all further experiments, therefore, characterizations were carried out using the catalyst coated titanium mesh working electrode.

### **4.3 Binary metal oxides as anode catalysts for solid polymer electrolyte electrolyzers**

Secondary metals (Sn, Ru, Ta and Pd) were carefully selected based on both a literature study and experimental results (as discussed in Chapter 2). Four binary

metal oxides were developed using the optimized synthesis conditions. The four binary metal oxides were studied to identify the best/most efficient catalyst for electrolysis.

#### **4.3.1 Ir-Ru mixed oxides as anode catalysts**

Ir-Ru mixed oxides have been studied quite extensively and there is much information available in the literature (as discussed in Section 2.2.3). It is known that the addition of RuO<sub>2</sub> to IrO<sub>2</sub> improves the catalytic activity of IrO<sub>2</sub> and the addition of IrO<sub>2</sub> to RuO<sub>2</sub> improves the stability of RuO<sub>2</sub> [49]. In this study Ir-Ru mixed oxides were prepared by varying the composition of ruthenium from 5 to 30 mol %. Chronoamperometry (Figures 4.14 and 4.15) revealed a maximum catalytic activity for Ir<sub>(0.7)</sub>Ru<sub>(0.3)</sub>O<sub>2</sub> at 1.8 V. The catalytic activity of Ir<sub>(0.7)</sub>Ru<sub>(0.3)</sub>O<sub>2</sub> was about 5.4 times greater than that of the commercial IrO<sub>2</sub> catalyst. An immediate increase in catalytic activity was observed with the addition of ruthenium. The most significant increase in catalytic activity was observed for the addition of 5 mol % ruthenium, followed by only minimal increases in catalytic activity for the addition of 10–30 mol % Ru. The addition of 5 mol % ruthenium resulted in an increase in catalytic activity of about 4.7 times greater compared to that of the commercial IrO<sub>2</sub> catalyst. This increased to about 5.4 times greater for Ir<sub>(0.7)</sub>Ru<sub>(0.3)</sub>O<sub>2</sub>. However, considering that IrO<sub>2</sub> is 2–3 times more expensive than RuO<sub>2</sub> [60], additions up to 30 mol % Ru would result in a significant overall cost benefit. The addition of RuO<sub>2</sub> to IrO<sub>2</sub> is assumed to have no significant effect on the electronic resistivity since the two oxides have similar electronic conductivities, as was noted earlier for Ir-Ru oxides [1].

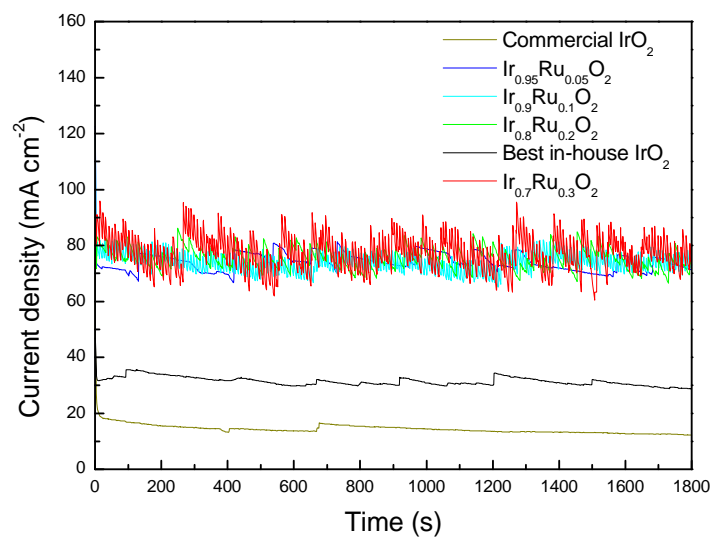


**Figure 4.14: Catalytic activity of Ir-Ru mixed oxides, commercial and best in-house IrO<sub>2</sub> at 1.8V.**

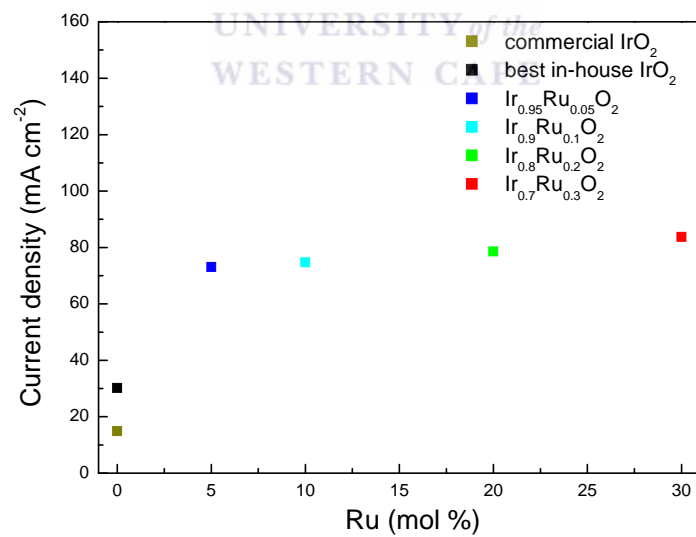


**Figure 4.15: Peak catalytic activity of Ir-Ru mixed oxides, commercial and best in-house IrO<sub>2</sub> at 1.8V.**



The XRD analysis of  $\text{Ir}_{(0.7)}\text{Ru}_{(0.3)}\text{O}_2$  (Figure 4.16) revealed a rutile oxide phase containing both amorphous and crystalline phases. Although it is known that  $\text{IrO}_2$  and  $\text{RuO}_2$  can form stable solid solutions [62], the presence of multiple rutile phases cannot be ruled out [17]. The Hume–Rothery theory states that it is possible to form a continuous solid solution of  $\text{IrO}_2$  and  $\text{RuO}_2$ , where  $\text{Ru}^{4+}$  and  $\text{Ir}^{4+}$  share the same site on the cationic sublattice of a tetragonal (rutile-like) phase [62]. A higher degree of crystallinity was observed for  $\text{Ir}_{0.7}\text{Ru}_{0.3}\text{O}_2$  than the best in-house  $\text{IrO}_2$  catalyst, which is consistent with  $\text{RuO}_2$  crystallizing at a lower temperature than  $\text{IrO}_2$  [17, 63]. Using the Scherrer formula, the average particle size of  $\text{Ir}_{(0.7)}\text{Ru}_{(0.3)}\text{O}_2$  was calculated to be 11 nm, which may be due to the higher degree of crystallization of  $\text{RuO}_2$ .

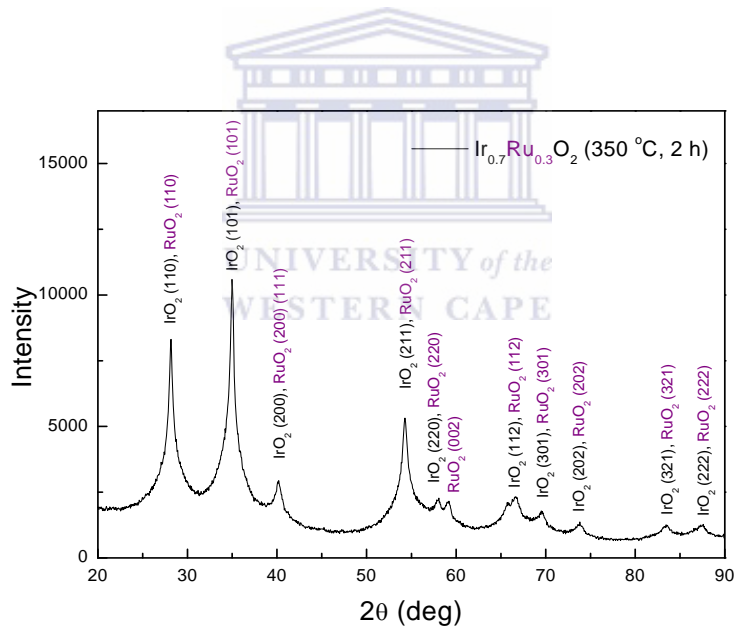


Figure 4.16: XRD patterns of  $\text{Ir}_{0.7}\text{Ru}_{0.3}\text{O}_2$  [59, 61].

SEM (Figure 4.17) revealed a smoother and more uniform surface than for IrO<sub>2</sub> (Figure 4.11). As the composition of ruthenium increased from 5 to 30 mol % there was an increase in uniformity. EDS analysis revealed that the bulk composition was close to the desired composition and that the distribution of the metals was quite uniform. TEM analysis of Ir<sub>0.7</sub>Ru<sub>0.3</sub>O<sub>2</sub> (Figure 4.18) revealed nanosized particles with regions of both low and high crystallinity. TEM revealed nanosized particles with the average particle size for the Ir<sub>0.7</sub>Ru<sub>0.3</sub>O<sub>2</sub> sample being 5 nm (much smaller than previously calculated). The particle sizes obtained from TEM were more in line with the catalytic activity revealed by chronoamperometry.

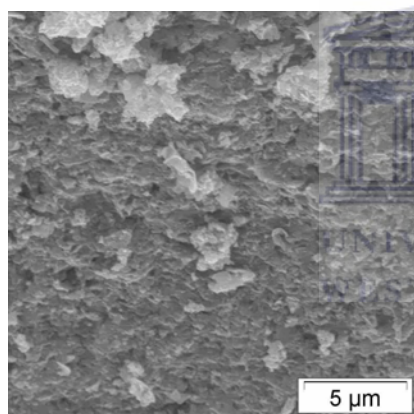


Figure 4.17: SEM image of Ir<sub>0.7</sub>Ru<sub>0.3</sub>O<sub>2</sub>.

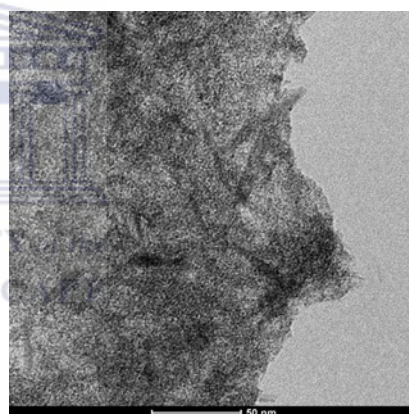


Figure 4.18: TEM image of Ir<sub>0.7</sub>Ru<sub>0.3</sub>O<sub>2</sub>.

Scale: 50 nm

### 4.3.2 Ir-Sn mixed oxides as anode catalysts

The addition of tin to iridium had been researched quite extensively by various groups [18, 51]. Ir-Sn mixed oxides are known to have similar activity to Ir-Ru mixed oxides but have an additional advantage due to the low cost of tin. Ir-Sn mixed oxides were prepared by varying the composition of tin from 5 to 30 mol %. Chronoamperometry (Figures 4.19 and 4.20) revealed a maximum catalytic activity for Ir<sub>(0.9)</sub>Sn<sub>(0.1)</sub>O<sub>2</sub> at 1.8

V The catalytic activity of  $\text{Ir}_{(0.9)}\text{Sn}_{(0.1)}\text{O}_2$  was about 5 times greater than that of the commercial  $\text{IrO}_2$  catalyst. Results clearly showed that the addition of tin to iridium resulted in improved catalytic activity, and would also result in an overall cost benefit considering the relative prices of iridium and tin [25]. Figure 4.19 shows that the Ir-Sn mixed oxides were quite stable over the 30 minutes electrolysis period at 1.8 V, however, long term stability could not be determined from such a short experimental period. Marshall *et al.* [25, 46] found that for the system  $\text{Ir}_x\text{Sn}_{1-x}\text{O}_2$  the active surface area was proportional to the iridium content of the oxide and that for tin additions (up to 20–30 mol %) the total available area only decreased by 10–15%. The decrease in catalytic activity for tin additions less than 10 mol % could be attributed to the decrease in the active surface area due to the formation of larger particles.

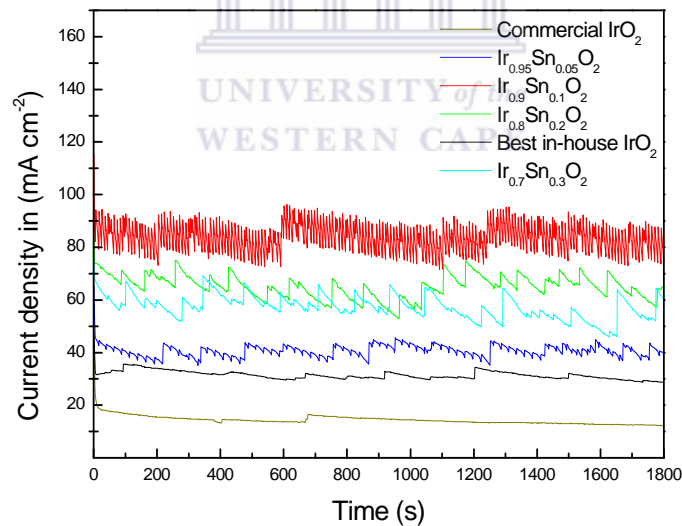


**Figure 4.19: Catalytic activity of Ir-Sn mixed oxides, commercial and best in-house  $\text{IrO}_2$  at 1.8V.**

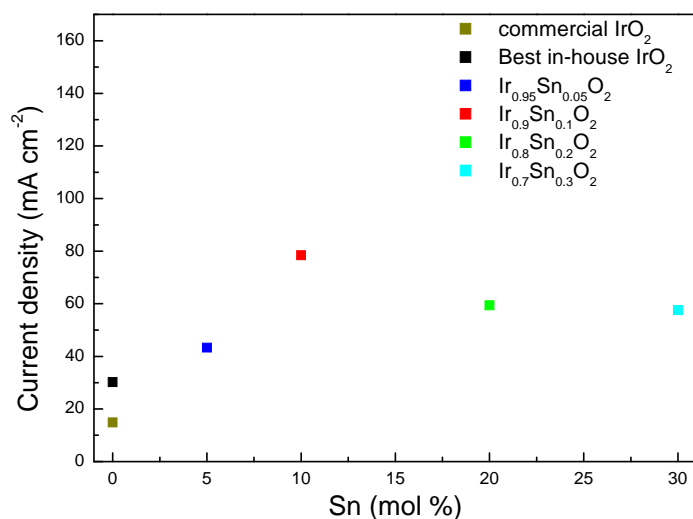


**Figure 4.20: Peak catalytic activity of Ir-Sn mixed oxides, commercial and best in-house IrO<sub>2</sub> at 1.8V.**

Zhang *et al.* [45] prepared SnO<sub>2</sub> via the Adams fusion method and obtained only a 95% yield at 350 °C. This could suggest that during the preparation of the Ir-Sn mixed oxides not all of the tin precursors were converted to SnO<sub>2</sub>. As the addition of tin was increased to 30 mol % the percentage of tin precursor converted to SnO<sub>2</sub> could possibly have decreased, resulting in the decreased catalytic activity when the tin additions were less than 10 mol %.

XRD analysis of Ir<sub>0.9</sub>Sn<sub>0.1</sub>O<sub>2</sub> (Figure 4.21) revealed a rutile-type oxide, however, it appeared that two separate phases were obtained rather than a single solid solution phase. This was suggested by the absence of clearly defined single peaks. The peaks appeared to be overlapping each other, thereby also decreasing the accuracy of the Scherrer formula for average particle size determination. However, using the Scherrer formula the average particle size of Ir<sub>0.9</sub>Sn<sub>0.1</sub>O<sub>2</sub> was determined to be 6 nm. Marshall

*et al.* [18] used profiling of the XRD patterns, which suggests that the XRD patterns were a mixture of two highly dispersed rutile oxide phases. Since the peaks were so broad an accurate determination of the structure was also not possible. The presence of multiple phases and the lack of a single solid solution phase were suggested to arise from the poor interaction of the precursors during the initial stages of the reaction [18]. It was assumed that SnO<sub>2</sub> formed first since there is a significant difference in  $\Delta G_f^0$  for IrO<sub>2</sub> and SnO<sub>2</sub> (-510 kJ mol<sup>-1</sup> [18, 65] and -186.5 kJ mol<sup>-1</sup> [18, 66], respectively).

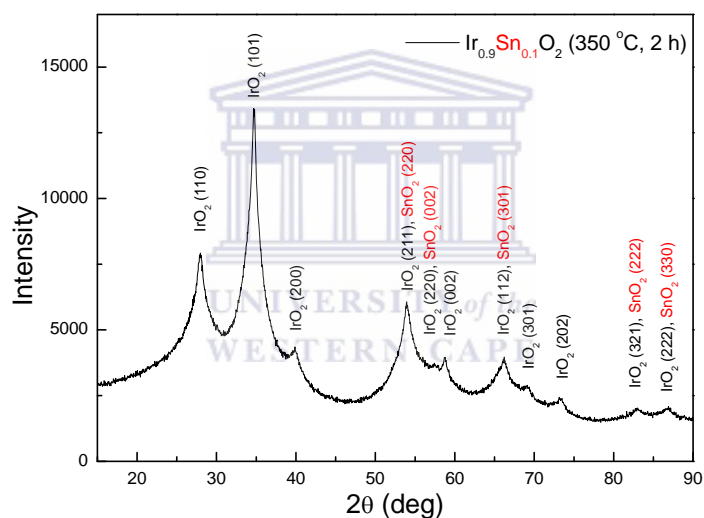


**Figure 4.21: XRD patterns of Ir<sub>0.9</sub>Sn<sub>0.1</sub>O<sub>2</sub> [59, 64].**

SEM analysis of Ir<sub>0.9</sub>Sn<sub>0.1</sub>O<sub>2</sub> (Figure 4.22) revealed morphology different to that of the in-house IrO<sub>2</sub> catalysts; no flake-like particles were observed. No significant changes in morphology were observed as the composition of tin was increased from 5 to 30 mol %. EDS analysis revealed that the bulk composition was close to the desired composition and that the distribution of the metals was quite uniform. TEM analysis of Ir<sub>0.9</sub>Sn<sub>0.1</sub>O<sub>2</sub> (Figure 4.23) revealed nanosized particles with regions of both low and

high crystallinity. It is known from literature [18, 46] that the particle sizes increase as the tin content is increased. TEM analysis revealed nanosized particles, with the average particle size for the  $\text{Ir}_{0.9}\text{Sn}_{0.1}\text{O}_2$  sample being 5 nm.

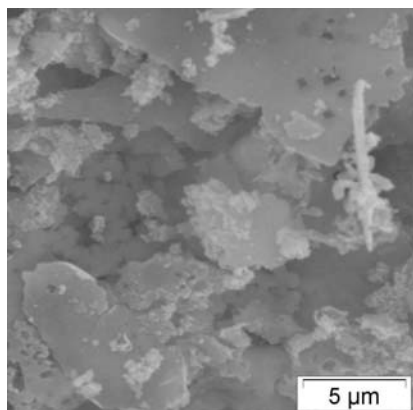


Figure 4.22: SEM image of  $\text{Ir}_{0.9}\text{Sn}_{0.1}\text{O}_2$ .

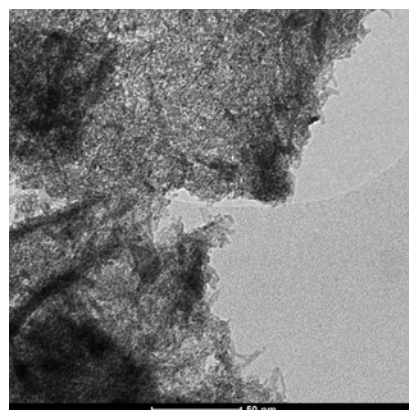


Figure 4.23: TEM image of  $\text{Ir}_{0.9}\text{Sn}_{0.1}\text{O}_2$ .

Scale: 50 nm

### 5.3.3 Ir-Ta mixed oxides as anode catalysts

$\text{IrO}_2\text{-Ta}_2\text{O}_5$  in the form of DSAs is well established in various electrochemical industries [1]. Tantalum oxide is added because of its high activity and stability in acidic media [17]. In this study Ir-Ta mixed oxides were prepared by varying the composition of tantalum from 5 to 30 mol %. Chronoamperometry (Figures 4.24 and 4.25) revealed a maximum catalytic activity for  $\text{Ir}_{(0.8)}\text{Ta}_{(0.2)}\text{O}_x$  at 1.8 V. The catalytic activity of  $\text{Ir}_{(0.8)}\text{Ta}_{(0.2)}\text{O}_x$  was about 3.4 times greater than that of the commercial  $\text{IrO}_2$  catalyst. Marshall *et al.* [17] found that upon the addition of  $\text{TaO}_x$  to  $\text{IrO}_2$  the resistivity increased by 2 orders of magnitude by the time the composition reached  $\text{Ir}_{(0.7)}\text{-Ta}_{(0.3)}\text{O}_x$ , since tantalum oxides are normally nonconductive. Although  $\text{Ir}_{(0.7)}\text{Ta}_{(0.3)}\text{O}_x$  was found to be more active than  $\text{IrO}_2$ , the reason for its activity being much lower compared to the other binary metal oxides studied may be due to the increase in electronic resistance.

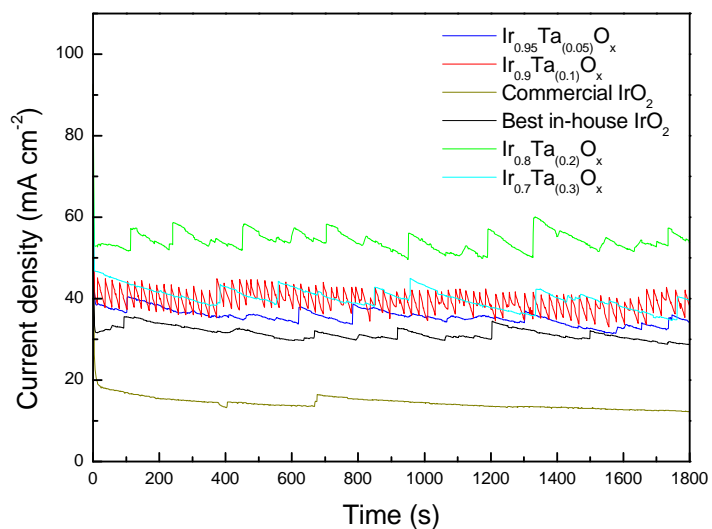


Figure 4.24: Catalytic activity of Ir-Ta mixed oxides, commercial and best in-house IrO<sub>2</sub> at 1.8V.

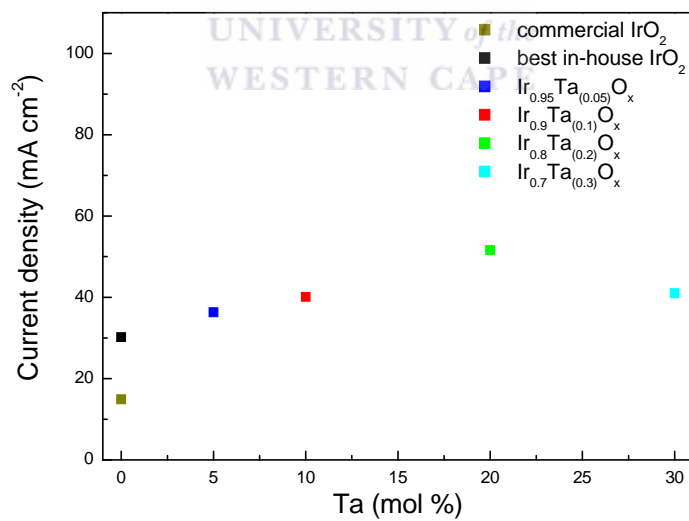


Figure 4.25: Peak catalytic activity of Ir-Ta mixed oxides, commercial and best in-house IrO<sub>2</sub> at 1.8V.

XRD analysis of  $\text{Ir}_{(0.8)}\text{Ta}_{(0.2)}\text{O}_x$  (Figure 4.26) revealed a decrease in the (110) orientation of  $\text{IrO}_2$  and a slight increase in the (002) (one of the non-close-packed planes of the Ir atom) orientation, which is consistent with what is reported in the literature [54, 67]. This could be explained by the stabilization effect that tantalum has on the iridium component in the non-close-packed plane [54]. XRD analysis further revealed a rutile structure with the absence of a single oxide phase, as indicated by the broad overlapping peaks. An average particle size assessment for  $\text{Ir}_{(0.8)}\text{Ta}_{(0.2)}\text{O}_x$  using the Scherrer formula was difficult due to the broad overlapping peaks. The broad overlapping peaks were indicative of low crystallinity. The addition of  $\text{Ta}_2\text{O}_5$  suppressed the crystallization of  $\text{IrO}_2$  [1], accounting for the low crystallinity. Tantalum was found to be present in the +5 oxidation state; consistent to what is reported in the literature [17].

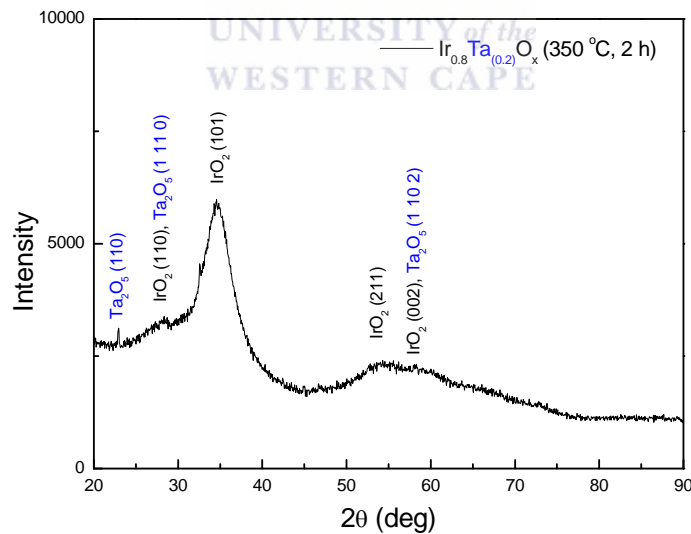


Figure 4.26: XRD patterns of  $\text{Ir}_{(0.8)}\text{Ta}_{(0.2)}\text{O}_x$  [59, 68].



SEM analysis revealed no significant change in morphology of the Ir-Ta mixed oxides as the tantalum composition was varied from 5 to 30 mol %. TEM analysis of  $\text{Ir}_{(0.8)}\text{Ta}_{(0.2)}\text{O}_x$  (Figure 4.28) revealed uniformly distributed nanosized particles. TEM revealed the average particle size for the  $\text{Ir}_{(0.8)}\text{Ta}_{(0.2)}\text{O}_x$  sample to be 3.5 nm. Rasten [1], using the Adams fusion method, found that the most important enhancing effect that the addition of the tantalum species had was mainly related to the reduction of the crystallite size.

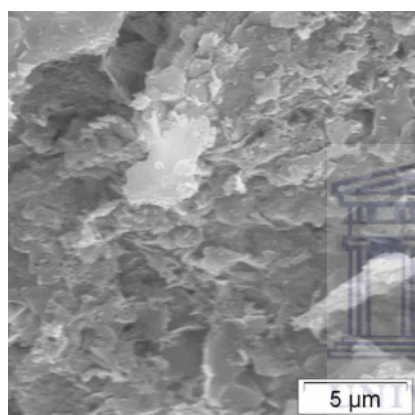


Figure 4.27: SEM image of  $\text{Ir}_{(0.8)}\text{Ta}_{(0.2)}\text{O}_x$ .

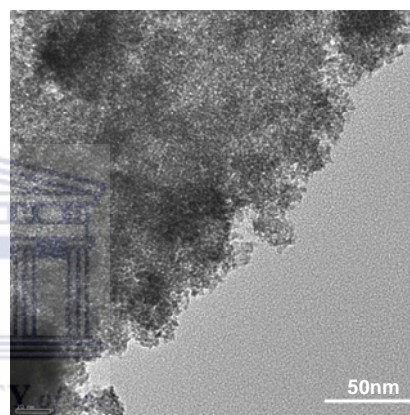


Figure 4.28: TEM image of  $\text{Ir}_{(0.8)}\text{Ta}_{(0.2)}\text{O}_x$ .

Scale: 50 nm

#### 4.3.4 Ir-Pd mixed oxides as anode catalysts

Palladium is known to exhibit high catalytic activity towards several electrochemical processes. Palladium has the unique ability to absorb hydrogen under ambient conditions [55, 69]; hydrogen occupies interstitial sites in the palladium lattice resulting in an expansion of the lattice [70, 71]. Palladium is known to be a good catalyst for the hydrogen dissociation reaction [72] and is also known to have excellent proton conductivity [73]. Palladium improves the charge/discharge characteristics of metal hydride electrodes; an effect attributed to the catalytic effect of palladium on the charge transfer step of hydriding and dehydriding reactions

occurring at the electrode surface [74]. In most oxidation reactions involving palladium the active phase is palladium oxide [75]. These characteristics of palladium have made it an interesting material to be researched as anode catalyst for the SPE electrolyser. Very little has been reported on the use of palladium as anode catalyst for SPE water electrolysis. This section focused on Ir-Pd mixed oxides used as anode catalysts for the SPE electrolyser. Ir-Pd mixed oxides were prepared by varying the composition of palladium from 5 to 30 mol %.

Chronoamperometry (Figures 4.29 and 4.30) revealed a maximum catalytic activity for  $\text{Ir}_{(0.7)}\text{Pd}_{(0.3)}\text{O}_x$  at 1.8 V. The catalytic activity of  $\text{Ir}_{(0.7)}\text{Pd}_{(0.3)}\text{O}_x$  (where x is undefined and further analysis such as XPS is necessary) was about 5 times greater than that of commercial  $\text{IrO}_2$  catalyst. Although no increase in catalytic activity was observed for the addition of 5 mol % palladium, a steady increase was observed as the composition of palladium was increased from 10 to 30 mol %.

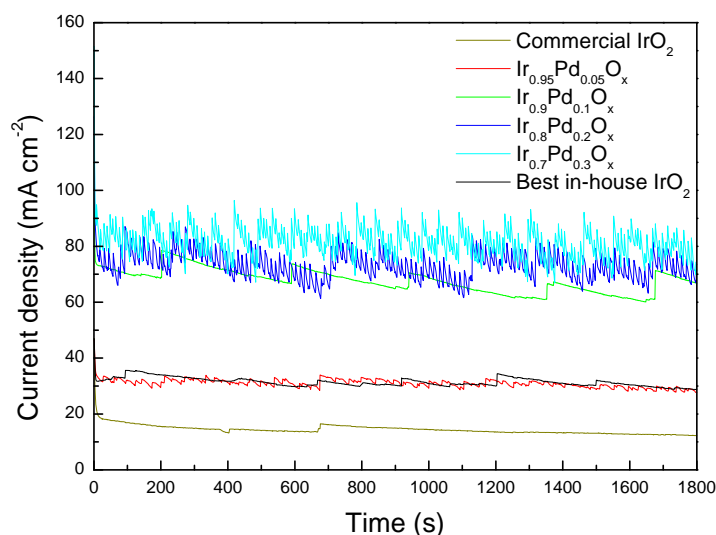


**Figure 4.29: Catalytic activity of Ir-Pd mixed oxides, commercial and best in-house IrO<sub>2</sub> at 1.8V.**

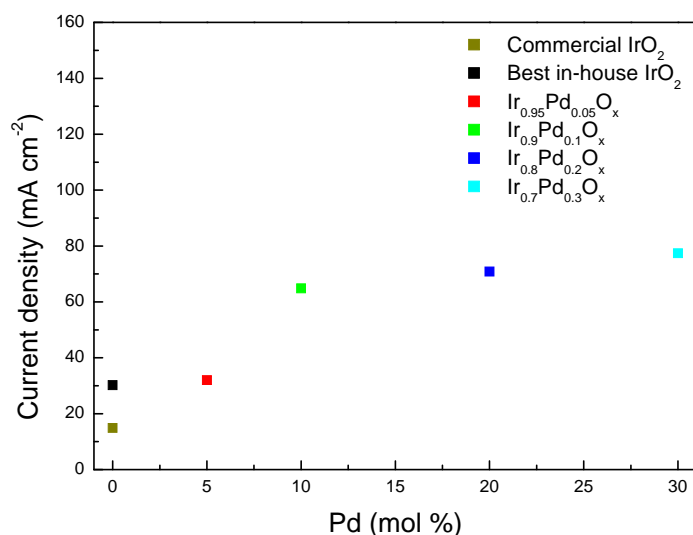


**Figure 4.30: Peak catalytic activity of Ir-Pd mixed oxides, commercial and best in-house IrO<sub>2</sub> at 1.8V.**

The increase in catalytic activity with the increase in palladium composition seems to attain a plateau above 10 mol %. Although it is too early to comment on the mechanism by which the palladium component increased the catalytic activity of IrO<sub>2</sub>, a possible explanation could be related to the excellent proton conducting properties of palladium. During the OER the removal of protons from the palladium active sites probably occurs at a much faster rate, thus increasing the availability of the active sites and thereby enhancing catalytic activity.

Shriner and Adams [56] found that complete conversion of the palladium precursor occurs at 500 °C. Thus the preparation conditions of the Ir-Pd mixed oxides could have had an effect on the activity of the catalyst. However it was established in Section 4.1.1 that at 500 °C a high degree of crystallization of IrO<sub>2</sub> takes place, which negatively affected the activity of the catalyst. A possible solution to obtain the best

preparation conditions for the Ir-Pd mixed oxides could be to separately prepare the two metal oxides, followed by mixing.

XRD analysis of  $\text{Ir}_{(0.7)}\text{Pd}_{(0.3)}\text{O}_x$  (Figure 4.31) revealed that palladium is present in both the +2 and +4 oxidation states. Compounds containing palladium in an oxidation state higher than +2 are few, and are usually prepared under elevated oxygen pressure [76]. XRD also revealed an increase in crystallinity as the composition of palladium was varied from 5 to 30 mol%. This is consistent with the literature [56], since palladium was found to be crystalline and had a square planar arrangement for PdO [76]. The presence of  $\text{PdO}_2$  is unclear since this compound normally decomposes to PdO at temperatures above 200 °C, particularly when it comes into contact with water.

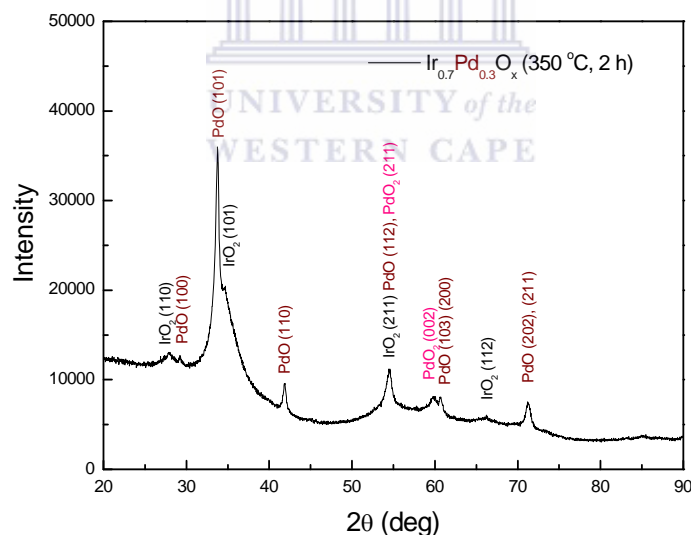


Figure 4.31: XRD patterns of  $\text{Ir}_{(0.7)}\text{Pd}_{(0.3)}\text{O}_x$  [59, 77, 78].

SEM analysis revealed no significant change in morphology of the Ir-Pd mixed oxides as the composition of palladium was varied from 5 to 30 mol %. TEM analysis of  $\text{Ir}_{(0.7)}\text{Pd}_{(0.3)}\text{O}_x$  (Figure 4.33) however revealed some interesting details, of which the

square and oval shaped particles were most obvious. The square shaped particles were probably due to the square planar arrangement of PdO. These particles were absent for the  $\text{Ir}_{(0.95)}\text{Pd}_{(0.05)}\text{O}_x$  sample and only formed as the composition of palladium was increased. Thus the significant increase in catalytic activity could be attributed to the presence of these square and oval shaped PdO particles. The  $\text{Ir}_{(0.7)}\text{Pd}_{(0.3)}\text{O}_x$  sample appeared to contain an amorphous region rich in  $\text{IrO}_2$  with particle sizes less than 10 nm and the large crystalline PdO particles that had particle sizes up to 75 nm. It is unclear how these large particles improved the catalytic activity of  $\text{IrO}_2$  towards the OER since an increase in particle size is normally associated with an increase in electronic resistance [1] and a decrease in the available active surface area [46]. Further investigation is necessary to determine the mechanism by which PdO contributes to the increase in catalytic activity of  $\text{IrO}_2$ .

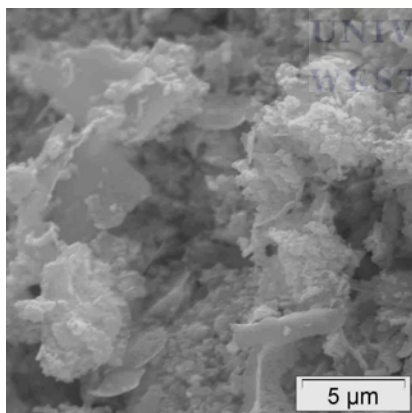


Figure 4.32: SEM image of  $\text{Ir}_{(0.7)}\text{Pd}_{(0.3)}\text{O}_x$ .

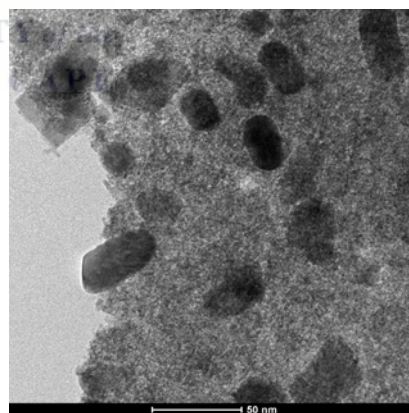


Figure 4.33: TEM image of  $\text{Ir}_{(0.7)}\text{Pd}_{(0.3)}\text{O}_x$ .

Scale: 50 nm

#### 4.3.5 Summary of the best catalysts

Figure 4.34 clearly shows that the Ir-Ru mixed oxide had the highest catalytic activity as anode catalyst for the SPE electrolyser over the electrolysis period used in this

study. All the catalysts showed considerable stability at 1.8 V and over the electrolysis period of 30 minutes. Ir-Pd and Ir-Sn mixed oxides showed similar activity to that of Ir-Ru mixed oxides. Considering the cost of tin, compared to ruthenium, tin seems an ideal candidate in terms of both cost and activity.

It is well known that the long term stability of the catalysts is crucial for commercial purposes. The catalysts reported here were studied only for half an hour, which do not necessarily give a clear indication regarding their long term stability. Future studies should therefore focus on studying the long term stability of these catalysts and their activity and stability in a SPE electrolyser.

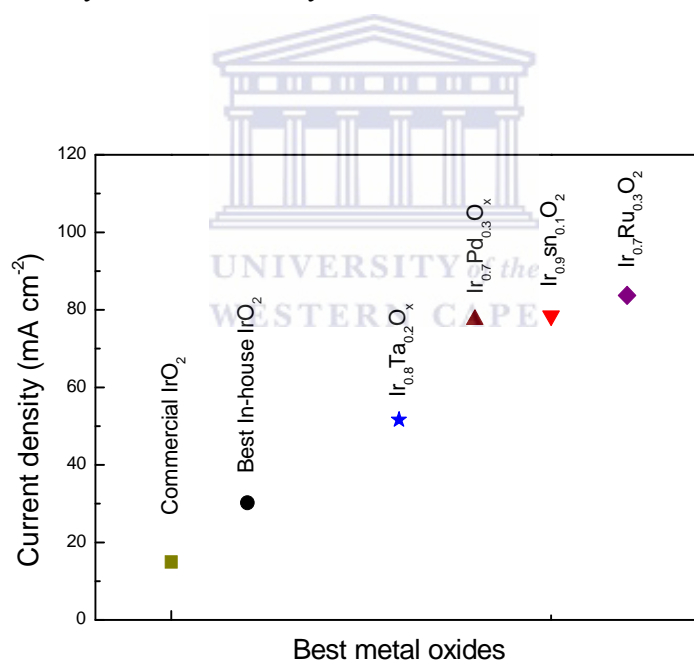
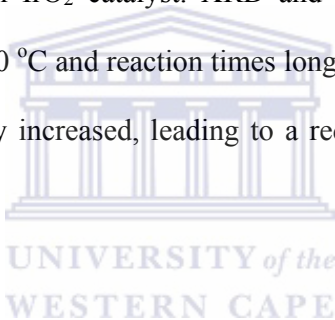


Figure 4.34: Peak catalytic activity of the best metal oxide catalysts at 1.8V.

## **Chapter 5: Conclusions and recommendations**

### **5.1 Conclusions**

Four binary metal oxides based on IrO<sub>2</sub> as well as an in-house unsupported IrO<sub>2</sub> were successfully prepared and optimized by adapting the Adams fusion method. Secondary metals (Sn, Ru, Ta and Pd) were selected after both a literature survey and experimental studies. The activities of the metal oxides were determined using half-cell studies. Optimum conditions for the preparation of unsupported IrO<sub>2</sub> catalysts were found to be 350 °C and 2 hours, which led to catalysts with twice the activity of the ‘state-of-art’ commercial IrO<sub>2</sub> catalyst. XRD and TEM analyses revealed that when temperatures above 350 °C and reaction times longer than 2 hours were used the particle size and crystallinity increased, leading to a reduction in the activity of the metal oxides.



All the binary metal oxides synthesized in this study showed improved catalytic activity compared to the unsupported IrO<sub>2</sub> catalyst. The best activity was exhibited by Ir<sub>0.7</sub>Ru<sub>0.3</sub>O<sub>2</sub>, which had a catalytic activity more than five times better than that of the ‘state-of-art’ commercial IrO<sub>2</sub> catalyst. Ir-Pd mixed oxides also proved to be highly efficient as anode catalysts for SPE electrolyzers. XRD and TEM analyses revealed that the Ir-Pd mixed oxide compounds contained particles up to 75 nm in size. It is unclear how these large particles are beneficial to the activity of these catalysts and therefore further investigation is necessary. Ir-Ta mixed oxides showed the lowest improvement in catalytic activity of the binary systems. The addition of tantalum led to amorphous particles, as revealed by XRD. Besides the electrocatalytic nature of tantalum, the lack of crystallinity might be a reason for the low catalytic activity. Ir-

Sn mixed oxides also showed significant improvement in catalytic activity:  $\text{Ir}_{0.9}\text{Sn}_{0.1}\text{O}_2$  performed about 5 times better than the 'state-of-art' commercial  $\text{IrO}_2$  catalyst. The addition of tin was limited to 10 mol %, since a significant decrease in activity was observed as the composition of tin was increased. Considering the relative cost of the secondary metals compared to iridium and that the binary metal oxides systems led to improved activity compared to unsupported  $\text{IrO}_2$ , it can be concluded that a significant reduction in the cost of the SPE electrolyser can be achieved.

## **5.2 Recommendations**

Based on literature studies and results obtained in this study some recommendations regarding future work are suggested below:

- Further investigation of the Ir-Pd mixed oxide catalysts is necessary to determine the mechanism by which the palladium component improve the activity of  $\text{IrO}_2$  and to optimize the synthesis conditions to develop catalysts with even better catalytic activity.
- Although the binary metal oxide systems revealed improved activity (over short periods) the stability of these systems (over longer periods) may be quite different, thus the long term stability of these binary metal oxides needs to be investigated, especially as this is crucial for commercialization of the SPE electrolyser.
- The activity of the best catalyst needs to be evaluated in a SPE electrolysis cell.



## References

1. E. Rasten, Electrocatalysis in water electrolysis with solid polymer electrolyte, Ph.D. thesis, Norwegian University of Science and Technology (2001).
2. A.K. Akella, R.P. Saini, M.P. Sharma, *Renewable Energy* 34 (2009) 390–396.
3. R.C. Saxena, D.K. Adhikari, H.B. Goyal, *Renewable and Sustainable Energy Reviews* 13 (2009) 169–178.
4. J.C. Ganley, *International Journal of Hydrogen Energy* 34 (2009) 3604–3611.
5. Energy Research Laboratory, Quantum Sphere Incorporation, Santa Ana, Highly efficient hydrogen generation via water electrolysis using nanometal electrodes (2006).
6. T.N. Veziroğlu, S. Şahin, *Energy Conversion and Management* 49 (2008) 1820–1831.
7. J.D. Holladay, J. Hu, D.L. King, Y. Wang, *Catalysis Today* (2008).
8. Investire-network, WP Report, Storage technology report, Investigation on storage technologies for intermittent renewable energies: Evaluation and recommended R&D strategy (30–06–2003).
9. D. Das, T.N. Veziroglu, *International Journal of Hydrogen Energy* 26 (2001) 13–18.
10. A. Ursúa, L. Marroyo, E. Gubía, L.M. Gandía, P.M. Diéguez, P. Sanchis, *International Journal of Hydrogen Energy* 34 (2009) 3221–3233.
11. B. Borresen, G. Hagen, R. Tunold, *Electrochimica Acta* 47 (2002) 1819–1827.
12. S.D. Ebbesen, M. Mogensen, *Journal of Power Sources* 193 (2009) 349–358.
13. V. Utgikar, T. Thiesen, *International Journal of Hydrogen Energy* 31 (2006) 939–944.
14. M.A. Laguna-Bercero, S.J. Skinner, J.A. Kilner, *Journal of Power Sources* 192 (2009) 126–131.
15. P. Millet, D. Dragoë, S. Grigoriev, V. Fateev, C. Etievant, *International Journal of Hydrogen Energy* 34 (2009) 4974–4982.
16. P. Millet, F. Andofatto, R. Durand, *International Journal of Hydrogen Energy* 21 (1996) 87–93.
17. A.T. Marshall, S. Sunde, M. Tsyarkin, R. Tunold, *International Journal of Hydrogen Energy* 32 (2007) 2320–2324.

18. A. Marshall, B. Børresen, G. Hagen, M. Tsypkin, R. Tunold, *Materials Chemistry and Physics* 94 (2005) 226–232.
19. S.A. Grigoriev, V.I. Porembsky, V.N. Fateev, *International Journal of Hydrogen Energy* 31 (2006) 171–175.
20. A. Deschamps, C. Etievant, V. Fateev, S. Grigoriev, A. Kalinnikov, P. Millet, V. Porembsky, C. Puyenchet, *Development of advanced PEM water electrolyzers, WHEC 16, Lyon France (13-16 June 2006)* 1–6.
21. Y. Zhang, C. Wang, N. Wan, Z. Liu, Z. Mao, *Electrochemistry Communications* 9 (2007) 667–670.
22. T. Tsuruda, National Research Institute of Fire and Disaster, 4–35–3 Jindaiji-Higashimachi, Chofu, Tokyo 182-8508, Japan, 21<sup>st</sup> ICDERS (23–27 July 2007).
23. J.H. Russel, L.J. Nutall, A.P. Fickett, General Electric Company, *Hydrogen generation by solid polymer electrolyte water electrolysis*, 24–40.
24. P. Choi, D.G. Bessarabov, R. Datta, *Solid State Ionics* 175 (2004) 535–539.
25. A. Marshall, B. Børresen, G. Hagen, M. Tsypkin, R. Tunold, *Energy* 32 (2007) 431–436.
26. F. Barbir, *Solar Energy* 78 (200) 661–669.
27. L. Sun, R. Ran, G. Wang, Z. Shao, *Solid State Ionics* 179 (2008) 960–965.
28. M. Eikerling, A.S. Loselevich, A.A. Kornyshev, *Fuel Cells* 4(3) (2004) 131.
29. R. Liu, W.H. Her, P.S. Fedkiw, *Journal of the Electrochemical Society* 139 (1) (1992) 15.
30. T. Sakai, Y. Kawami, H. Takenaka, E. Torikoi, *Journal of the Electrochemical Society* 137 (12) (1990) 3777.
31. E. Rasten, G. Hagen, R. Tunold, *Electrochimica Acta* 48 (2003) 3945–3952.
32. S.A. Grigoriev, P. Millet, S.V. Korobtsev, V.I. Porembskiy, M. Pepic, C. Etievant, C. Puyenchet, V.N. Fateev, *International Journal of Hydrogen Energy* (2009) 1–6.
33. Z. Ogumi, Z. Takehara, S. Yoshizawa, *Journal of the Electrochemical Society* 131 (1984) 769–773.
34. S. Trasatti, *Journal of Electroanalytical Chemistry* 39 (1972) 163.
35. B.E. Conway, G. Jerkiewicz, *Electrochimica Acta* 45 (2000) 4075–4083.
36. M.M. Jaksic, *Solid State Ionics* 136 (2000) 733.
37. S. Fierro, T. Nagel, H. Baltruschat, C. Comminellis, *Electrochemistry Communications* 9 (2007) 1969–1974.

38. J. Hu, J. Zhang, C. Cao, *International Journal of Hydrogen Energy* 29 (2004) 791–797.
39. F. Andolfatto, R. Durand, A. Michas, P. Millet, P. Stevens, *International Journal of Hydrogen Energy* 19 (1994) 421.
40. S. Trasatti (1990) Electrode kinetics and electrocatalysis of hydrogen and oxygen electrode reactions. The oxygen evolution reaction. In: Wendt H (ed) *Electrochemical hydrogen technologies*. Elsevier, Amsterdam, pp 104–135.
41. I. Krasil'shchikov, *Zhurnal Fizicheskoi Khimii* 37 (1963) 531.
42. M.E.G. Lyons, M.P. Brandon. *International Journal of Electrochemical Science* 3 (2008) 1425–1462.
43. J.C.K. Ho and D.L. Piron, *Journal of Applied Electrochemistry* 26 (1996) 515.
44. A. Marshall, B. Børresen, G. Hagen, S. Sunde, M. Tsyppkin, and R. Tunold, *Russian Journal of Electrochemistry* 42 (10) (2006) 1134–1140.
45. Y. Zhang, C. Wang, Z. Mao, N. Wang, *Materials Letters* 61 (2007) 1205–1209.
46. A. Marshall, B. Børresen, G. Hagen, M. Tsyppkin, R. Tunold, *Electrochimica Acta* 51 (2006) 3161–3167.
47. E. Slavcheva, I. Radev, S. Bliznakov, G. Topalov, P. Andreev, E. Budevski, *Electrochimica Acta* 52 (2007) 3889–3894.
48. L. Ma, S. Sui, Y. Zhai, *Journal of Power Sources* 177 (2008) 470–477.
49. J. Cheng, H. Zhang, G. Chen, Y. Zhang, *Electrochimica Acta* (2009).
50. A. Kuzmin, R. Kalendarev, J. Purans, D. Pailharey, *Iridium L<sub>3</sub>-edge and oxygen K-edge X-ray absorption spectroscopy of nanocrystalline iridium dioxide thin films*, *Proceedings of SPIE* 5122 (2003) 79–85.
51. C.P. De Pauli, S. Trasatti, *Journal of Electroanalytical Chemistry* 538–539 (2002) 145–151.
52. K. Katsiev, M. Batzill, L.A. Boatner, U. Diebold, *Surface Science* 602 (2008) 1699–1704.
53. H. Ma, C. Liu, J. Liao, Y. Su, X. Xue, W. Xing, *Journal of Molecular Catalysis A: Chemical* 247 (2006) 7–13.
54. J.M. Hu, H.M. Meng, J.Q. Zhang, C.N. Cao, *Corrosion Science* 44 (2002) 1655–1668.
55. M. Grden, M. Lukaszewski, G. Jerkiewicz, A. Czerwinski, *Electrochimica Acta* 53 (2008) 7583–7598.

56. R.L. Shriner, R. Adams, The preparation of palladous oxide and its use as a catalyst in the reduction of organic compounds, VI, Ph.D. thesis abstract, Chemical laboratory of the University of Illinois (1924) 1683–1693.
57. R. Adams, R.L. Shriner, Platinum oxides as a catalyst in the reduction of organic compounds. III, Preparation and properties of the oxide of platinum obtained by the fusion of chloroplatinic acid with sodium nitrate, Ph.D. thesis abstract, Chemical laboratory of the University of Illinois (1923) 2171–2179.
58. N. Toshima, T. Yonezawa, *New Journal of Chemistry* (1998) 1179–1201.
59. National Bureau of Standards (U.S.) Monogram 25 (4) (1965) 19.
60. C.P. De Pauli, S. Trassati, *Journal of Electroanalytical Chemistry* 396 (1995) 161–168.
61. J. Welton, G. McCarthy, ICDD Grant-in-Aid, North Dakota State University, USA (1989).
62. E. Balko, C. Davidson, *Journal of Inorganic Nuclear Chemistry* 42 (1980) 1778–1781.
63. A. Newkirk, D. McKee, *Journal of Catalysis* 11 (1968) 370–377.
64. J. Welton, G. McCarthy, *Powder Diffraction* 4 (1989) 156.
65. C. Mallika, A.E.S. Raj, K. Nagaraja, O. Sreedharan, *Thermochimica Acta* 371 (2001) 95.
66. S. Trasatti, G. Lodi, S. Trasatti, *Electrodes of conductive metallic oxides*, Elsevier Scientific Publishing Company, Amsterdam (1980) p 301.
67. J.M. Hu, J.X. Wu, H.M. Meng, D.B. Sun, Y.R. Zhu, D.J. Yang, *Transactions of Nonferrous Metals Society of China (English letters)* 10 (2000) 511.
68. S. Roth, J.L. Waring, S. Parker, *Journal of Solid State Chemistry* 2 (1970) 445.
69. G. Jimenez, E. Dillon, R. Miller, F. Massicotte, S. Nesbit, A. Craft, *Scripta Materialia* 59 (2008) 870–873.
70. P. Tripodi, N. Armanet, V. Asarisi, A. Avveduto, A. Marmigi, J. Darja Vinko, J. Biberian, *Physics Letters A* 373 (2009) 3101–3108.
71. F.A. Lewis, *Platinum Metals Review* 26 (2) (1982) 70.
72. L. Zaluski, A. Zaluska, P. Tessier, J.O. Ström-Olsen, R. Schulz, *Journal of Alloys and Compounds* 217 (1995) 295–300.
73. B. Baranowski, S.Y. Zaginaichenko, D.V. Schur (2008), *Carbon nanomaterials in clean hydrogen energy systems*, NATO Science for Peace and Security Series C: Environmental Security, Springer, pp 145

74. R.C. Ambrosio, E.A. Ticianelli, *Surface and Coatings Technology* 197 (2005) 215–222.
75. E.H. Voogt, A.J.M. Mens, O.L.J. Gijzeman, W.J. Geus, *Surface Science* 350 (1996) 21–31.
76. R.V. Panin, N.R. Khasanova, A.M. Abakumov, E.V. Antipov, G. Van Tendeloo, W. Schnelle, *Journal of Solid State Chemistry* 180 (2007) 1566–1574.
77. J. Welton-Holzer, G. McCarthy, ICDD Grant-in-Aid, North Dakota State University, Fargo, USA (1989)
78. L. Shaplygin, *Russian Journal of Inorganic Chemistry* (Eng. transl.) 23 (1978) 448.

